

# ALL LAMINAR SAILPLANES WITH LOW DRAG BOUNDARY LAYER SUCTION

by Werner Pfenninger

Presented at the XIX OSTIV Congress, Rieti, Italy (1985)

## FOREWORD

This report discusses the potential and the overall and detail design considerations of all-laminar LFC sailplanes. It is based on lectures given at the 18th OSTIV Conference in Hobbs, New Mexico, July 1983, and the convention of the Soaring Society of America in San Diego, California, March 1985.

Except for the lower Reynolds number range of LFC sailplanes many problems involved in the design of global range LFC airplanes, especially of a performance demonstration LFC airplane of unprecedented range, are identical to those of all laminar high performance LFC sailplanes. Therefore, this report may be of much more general interest than for LFC sailplanes only.

## A. INTRODUCTION

In the quest for better sailplane performance laminar flow has been extended on the wings. As laminar flow and transition is shifted further downstream, one runs into the problems of eliminating laminar separation bubbles on both wing surfaces for pressure drag minimization and ensuring a satisfactory turbulent rear pressure recovery, especially with fully turbulent flow on the wings (due to rain, etc.). Of course, thinner wings, structurally now feasible with graphite, can be designed for more extensive laminar flow, but more emphasis must then be put on small chord trailing edge cruise flap deflection to ensure an adequate low drag  $c_{L}$ -range. With increasing extent of natural laminar flow on the wings increasingly delicate measures are needed to eliminate laminar

separation bubbles on the wing surfaces. With their length Reynolds number of about 50,000 laminar separation bubbles extend over a relatively large percentage of the wing chord at sailplane Reynolds numbers. When the turbulent pressure rise immediately downstream of transition is very steep with particularly extensive natural laminar flow the laminar separation bubbles on the wing can easily cause a substantial increase in wing pressure- and profile drag at lower  $Re_c$ 's.

Various types of turbulator devices are now being used to control and suppress laminar separation bubbles on modern sailplanes. During the early 1940's the author has used turbulator bleed holes and rear facing surface steps for this purpose.<sup>1</sup> Tripping the boundary layer by means of boundary layer suction through a spanwise row of reasonably closely spaced suction holes (Goldsmith's experiments),<sup>2</sup> avoids turbulator device drag and thins at the same time the boundary layer at the start of the rear pressure rise to improve accordingly the turbulent rear pressure recovery. Thus, suction through a spanwise row of holes appears particularly attractive as a turbulator device, if a suction source is available.

Once one considers boundary layer suction for control and elimination of laminar separation bubbles, one might go a step further and increase suction to obtain more extensive laminar flow on the wings. Since the airplane lift-to-drag ratio increases most dramatically when the entire airplane is laminarized by means of low drag boundary layer suction, as shown by **Figure 1**, one might then be tempted to ask why not laminarize the entire wing surface further downstream by means of low drag boundary layer suction.

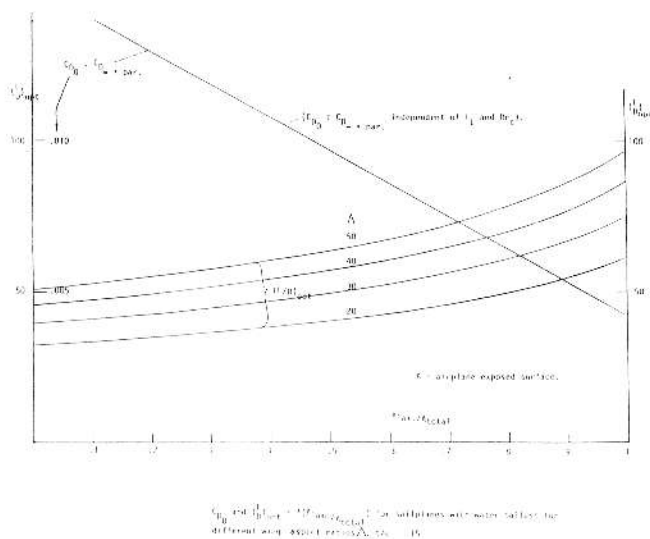


FIGURE 1 A.

Boundary layer suction on LFC sailplane wings is primarily needed in their rear pressure rise area to remove the particularly dangerous slowest innermost particles of the boundary layer in this area, which otherwise would separate to cause premature transition. At higher length Reynolds numbers, such as on a fuselage, boundary layer suction is needed to stabilize the laminar boundary layer and reduce the growth of amplified Tollmien-Schlichting (TS) type boundary layer disturbances and thereby extend laminar flow to much higher length Reynolds numbers.

The influence of boundary layer suction follows also from the boundary condition at the wall ( $y=0$ ) of the streamwise

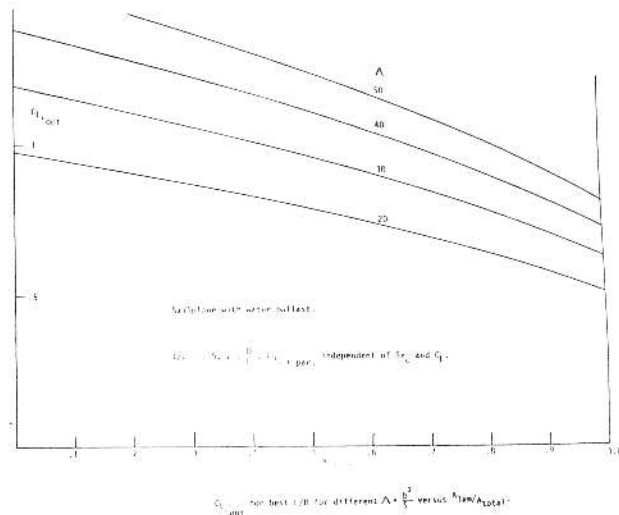


FIGURE 1 B.

boundary layer momentum equation:

$$v_0 \left( \frac{\partial u}{\partial y} \right)_0 = - \frac{1}{\rho} \frac{\partial p}{\partial x} + \left( \frac{\partial^2 u}{\partial y^2} \right)_0$$

To maintain Blasius type boundary layers

$$\left\{ \left( \frac{\partial^2 u}{\partial y^2} \right)_0 = 0 \right\}$$

in the rear pressure rise area of wings needs a suction velocity

$$v_0 = \frac{- \partial p / \partial x}{\rho \left( \frac{\partial u}{\partial y} \right)_0}$$

leading to the suction velocity ratio

$$\frac{v_0}{U_\infty} = -2.25 \times \frac{\partial c_p / \partial (x/c)}{1 - c_p} \times \frac{Re_\theta}{Re_c}$$

In the absence of pressure gradients

$$\frac{\partial p}{\partial x} = 0, \quad v_0 \left( \frac{\partial u}{\partial y} \right)_0 = \left( \frac{\partial^2 u}{\partial y^2} \right)_0, \quad \text{i.e.} \quad \left( \frac{\partial^2 u}{\partial y^2} \right)_0$$

is negative with suction ( $v_0 < 0$ ) to generate continuously convex boundary layer profiles, being more stable to TS-disturbances. The corresponding suction velocities are usually much smaller than those needed for suction laminarization in the rear pressure rise area of LFC wings and bodies.

Boundary layer suction is particularly effective in controlling the growth of amplified TS-vortices, as long as they are two-dimensional and not yet distorted three-dimensionally at larger amplitudes. Boundary layer suction is less effective in controlling the growth of boundary layer crossflow disturbances. Most difficult is the control of centrifugal type Taylor-Goertler boundary layer instability in regions of concave curvature on the wing and fuselage. The growth of Taylor-Goertler vortices can be minimized by turning the flow around through one or several concave "corners," instead of using a surface of continuous concave curvature.<sup>3</sup>

In addition, the substantially thinner boundary layer with low drag suction in the rear wing pressure rise area improves the effectiveness of a trailing edge cruise flap and aileron,<sup>5</sup> thereby increasing the low drag  $C_L$ -range and improving aileron control effectiveness and roll damping.

**Figure 2** shows the reduction of the wing profile drag  $C_{D\alpha}$  of a 14.5 per cent thick airfoil with increasing extent of lami-

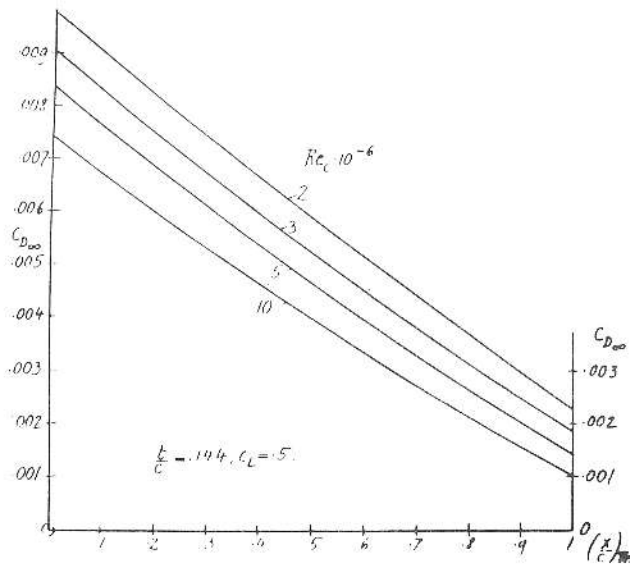


FIGURE 2

nar flow for different wing chord Reynolds numbers  $Re_c$ . Phenomenally low  $C_{D\infty}$  values appear feasible with full chord laminar flow by means of low drag suction, especially at higher  $Re_c$ 's, as confirmed experimentally in low turbulence tunnels as well as in flight. As an example Figure 3 shows  $C_{D\infty}$  versus  $Re_c$  for a 15 percent thick slotted laminar flow control (LFC) airfoil, designed by the author and tested in 1951 at the Langley TDT-tunnel.<sup>4</sup> Full chord laminar flow existed up to  $Re_c = 17.10^6$  with  $C_{D\infty min} = .0011$ , including the equivalent suction drag. With increasing  $Re_c$ 's,  $C_{D\infty}$  decreased in a similar manner as the drag of a laminar flat plate. Figure 3 includes drag results of the author's 17 percent thick slotted Zurich LFC airfoil with full chord laminar flow and  $C_{D\infty min} = .0023$  at  $Re_c = 2.3.10^6$ . The drag rise at higher  $Re_c$ 's is due to the high turbulence of the Zurich tunnel (0.4 percent). The 10 times lower turbulence level of the TDT-tunnel enabled full chord laminar flow up to correspondingly higher  $Re_c = 17.10^6$ . The weaker microscale turbulence of the atmosphere approximately doubles the laminar flow length Reynolds number of LFC surfaces in low turbulence tunnels.<sup>6</sup>

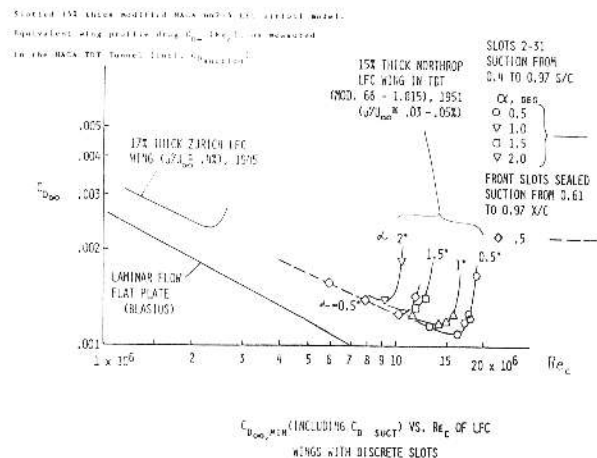
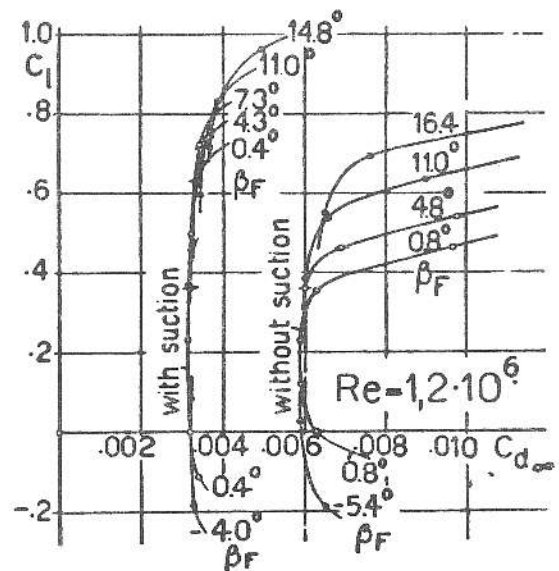
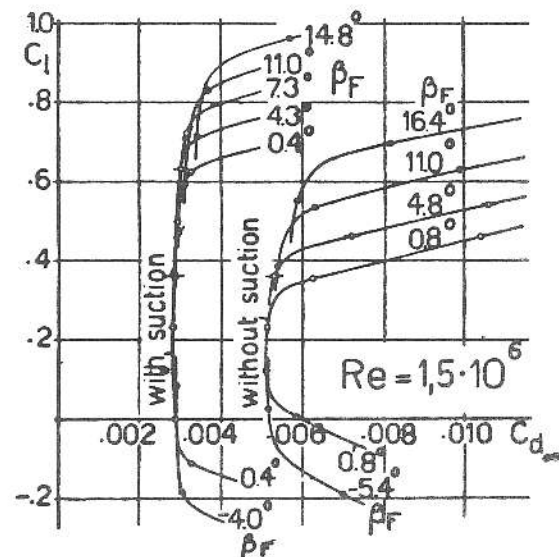
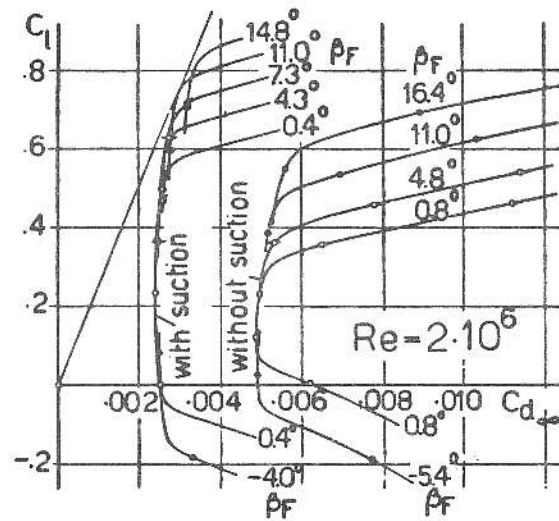


FIGURE 3



Profile polars  $c_l(c_{d\infty})$  without and with suction (including the equivalent drag due to the power of the suction fans) for different flap angles  $\beta_F$  and Reynolds Numbers,  $Re$ .

FIGURE 4

The effect of a small chord trailing edge cruise flap was investigated on the above mentioned 17 percent thick Zurich LFC airfoil (Figure 4), showing a substantially improved  $C_L$ -range over the corresponding nonsuction airfoil.<sup>5</sup>

Of interest for suction laminarization of the fuselage are low drag suction experiments on a 8:1 fineness ratio Reichardt type low drag suction body of revolution, designed by the author's LFC research group at Northrop and tested in the Ames 12-foot tunnel.<sup>7</sup> Distributed suction had been approached by suction through a large number of closely spaced fine slots, continuously removing the innermost slowest parts of the boundary layer. Full length laminar flow had been obtained on this LFC body up to a length Reynolds number  $Re_L = 58.10^6$ , with  $C_{Dmin} = .00026$  (based on body wetted area and including the equivalent suction drag, assuming acceleration of the suction air to undisturbed velocity with the same efficiency as the propulsive efficiency of the main propulsion system) (Figure 5). This drag is but insignificantly higher than the laminar friction drag of a flat plate and about 8 to 9 times lower than the turbulent flat plate skin friction at the same length Reynolds number. Up to  $30.10^6$  the equivalent body drag was essentially inversely proportional to

$$\sqrt{Re_c}$$

Of further interest for fuselage suction laminarization are Goldsmith's low drag suction experiments in juncture areas between a flat plate and a low drag suction wing. In these experiments Goldsmith had been able to maintain laminar flow by means of suction in the entire juncture area, even in the region of the plate downstream of the wing trailing edge in the presence of a purely viscous laminar wing wake (Figures 6 and 7).<sup>8</sup>

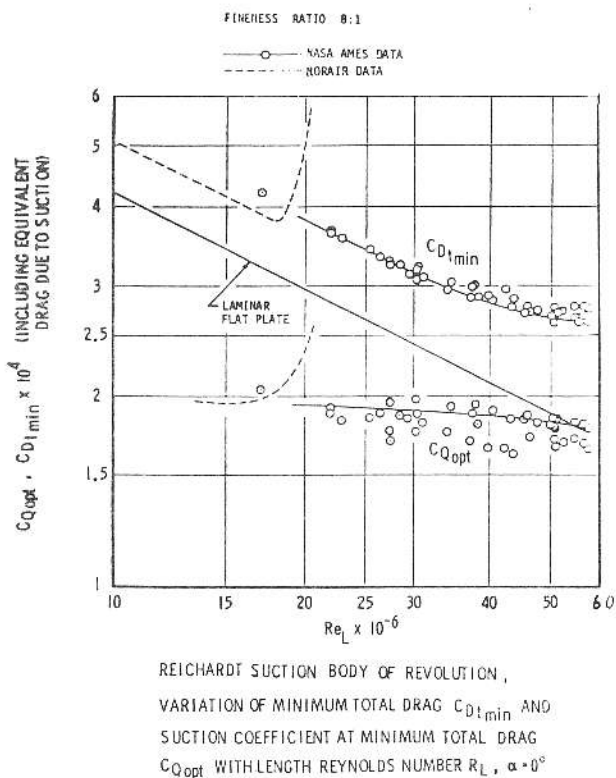
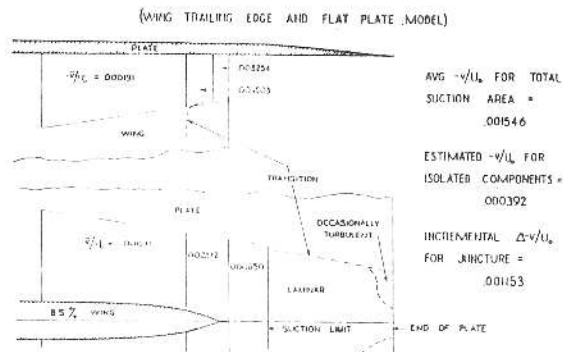


FIGURE 5



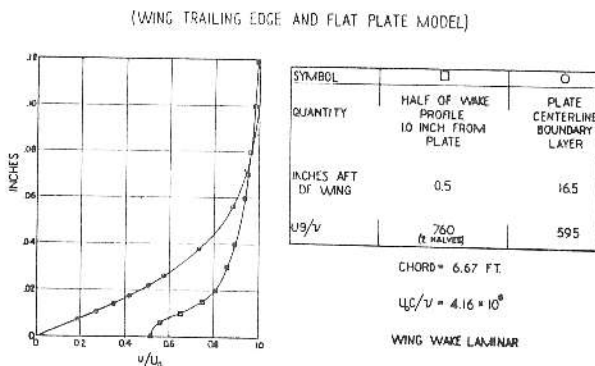
### SUCTION NEAR JUNCTURE

FIGURE 6

#### B. FORMULATION OF GOAL

If it should prove feasible to apply these results to a large span all laminar LFC sailplane with low drag suction an unusual aerodynamic performance would result, favoring dolphin type soaring, including flight in thermal waves,<sup>9</sup> and possible enabling static<sup>10</sup> as well as dynamic soaring in the jet-stream over large distances.<sup>11</sup> For such dynamic soaring in the jet-stream a large span is desirable to maximize  $L/D$  and  $V_{sink}$ . In his dynamic soaring flights in a low altitude shear layer in Australia Ingo Renner has shown the decisive superiority of the 24.5 meter Nimbus 3 over 15 meter sailplanes.

One might thus set as a bold goal the development of an all laminar LFC sailplane of around 30 meters span with low drag suction. This report describes overall and detail design considerations and the performance of such a machine; the problems involved and solutions to solve them; and how to build it. No question, such an LFC sailplane will be substantially more complex than a conventional one. The exceptional performance with  $(L/D)$  values close to 100 and especially the phenomenal high speed performance will justify the effort, especially since the experience gained with the development of such a high performance LFC sailplane can be applied to powered long range LFC airplanes, when special missions require an exceptional range performance.



### PROFILES BEHIND JUNCTURE

FIGURE 7. Boundary Layer

### C. OVERALL DESIGN CONSIDERATIONS

The design of a high performance LFC sailplane represents a compromise between many conflicting requirements. In contrast to sailplanes without suction the design of a LFC sailplane is strongly influenced by the desire to keep the complexity of the suction system (suction surface, suction-ducting and suction-drive) within bounds, at least for a first LFC sailplane.

To improve the glide ratio and minimum sink rate the span of high performance single seater sailplanes has steadily increased to 25 meters, possible by the use of advanced composites, until problems with aileron control, roll damping and adverse yaw set limits. Since boundary layer suction improves flap and aileron effectiveness substantially, aileron control and roll damping improve accordingly to allow increased wing spans, especially taking into account that the optimal speeds for  $(L/D)_{opt}$  and  $v_{sink\ min}$  are higher for all laminar LFC sailplanes as a result of the lower  $C_{L,opt}$  with the much lower wing profile drag and airplane parasitic drag. Furthermore, if it should prove feasible to approach  $(L/D)$ 's of the order of 100 with all laminar flow by means of suction dolphin type soaring becomes increasingly attractive; circling flight will then become less important.

With these considerations in mind a wing span of around 30 meters was tentatively chosen. After selecting the span the question arises concerning the choice of the wing aspect ratio or wing chord for a given absolute wing thickness, dictated by structural and aeroelastic considerations. The best glide ratio or minimum sink rate would be obtained by selecting the chord such that the wing operates close to the maximum section lift-to-drag ratio  $(C_L/C_{D\infty})$  (for a given absolute wing thickness) at the  $C_L$  for  $(L/D)_{max}$  or  $v_{sink\ min}$ . The question then arises concerning the profile drag polars  $C_L(C_{D\infty})$  for LFC airfoils of various thickness ratios  $t/c$ , operating at different  $C_L$ 's and  $Re_c$ 's. For a given wing thickness, i.e., constant structural weight for wing bending strength and a given flight speed, chord  $c$  and  $Re_c$  vary inversely proportional to  $t/c$ , while  $C_L$  is proportional to  $t/c$ . Under otherwise the same conditions

$$C_{D\infty} \sim \sqrt{\frac{1}{Re_c}}$$

in the Reynolds number range of sailplanes. With these considerations in mind the boundary layer development was analyzed for different cases, varying the airfoil thickness ratio  $t/c$  and  $C_L$  and the location of the start of the rear pressure rise on upper and lower surface. The Figures 8 and 9 show plots of the equivalent wing profile drag  $C_{D\infty}$  with and without losses in the suction ducting and suction drive system of LFC wings of different thickness ratios  $t/c$  and  $\bar{x}$  values, as obtained from these boundary layer development calculations with area suction and full chord laminar flow at  $Re_c = 2 \cdot 10^6$  and  $C_L = .5$ . ( $x$  is the location for the start of the rear pressure rise (average between both wing surfaces)). Included in figure 8 is the corresponding equivalent suction drag  $C_{D_s}$  assuming 100 percent efficiency for the suction compressor. As long as full chord laminar flow can be maintained the increase in  $C_{D\infty}$  with  $t/c$  at a given value of  $Re_c$  is surprisingly small, particularly for the case without losses in the suction ducting and suction drive system. Taking these losses into account increases the rise of  $C_{D\infty}$  with  $t/c$  (fig. 9).

In contrast to natural laminar flow airfoils without suc-

tion, the variation of  $C_{D\infty}$  versus the location

$\frac{x}{c}$   
C  
for the start of the rear pressure rise is small under otherwise the same conditions ( $C_L$ ,  $Re_c$ ,  $t/c$ ), as long as transition can be kept at the trailing edge by means of suction. LFC airfoils with a more rearward location of the pressure rise are slightly superior dragwise.

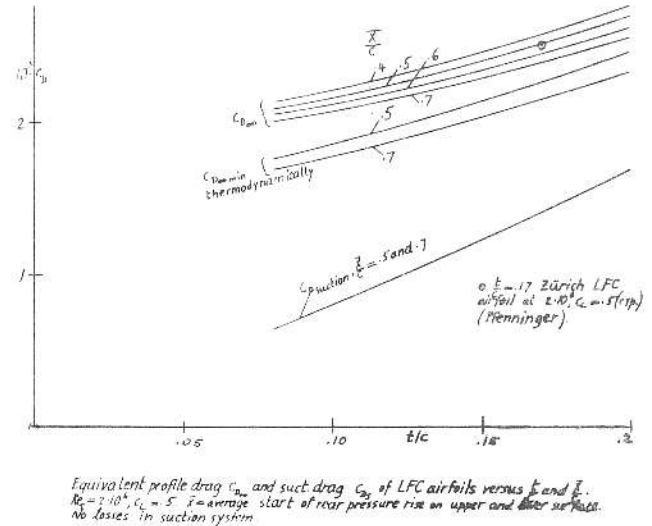


FIGURE 8

According to Ackeret,<sup>12</sup> and also reported by the author,<sup>1</sup> the equivalent profile drag of LFC airfoils can, in principle, be still further reduced by reaccelerating each boundary layer particle at the trailing edge individually to freestream velocity (fig. 8), thereby recovering the otherwise lost wake kinetic energy, as seen by an absolute observer. In practice, one might thus recover perhaps  $1/2$  to  $2/3$  of this wake kinetic energy. This appears easier at higher Reynolds numbers because of the relatively thinner boundary layers and the correspondingly smaller nondimensional suction rates  $v_0/U_\infty$ .

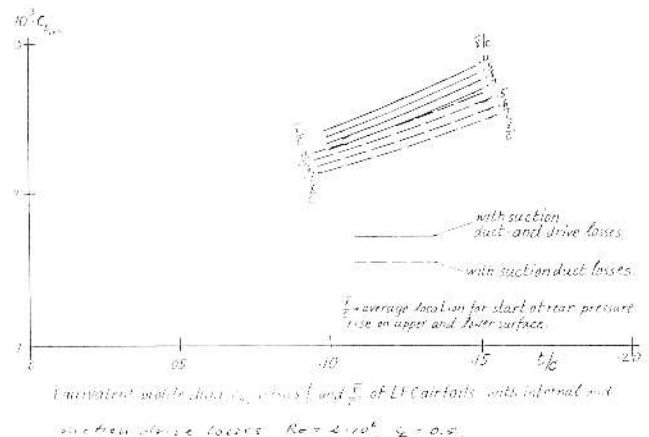
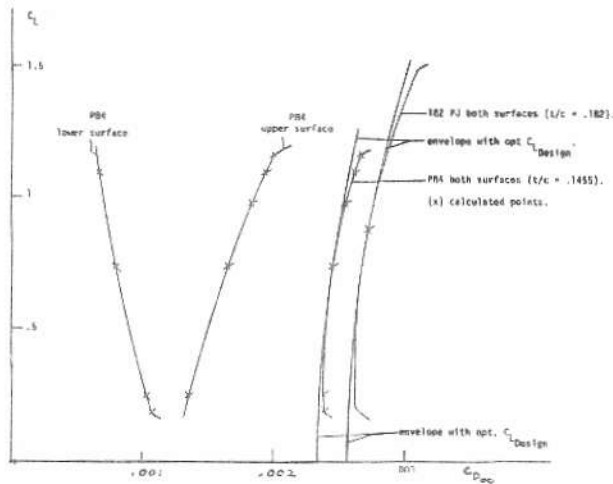


FIGURE 9

Figure 10 shows the variation of  $C_{D\infty}$  (without losses) versus  $C_L$  at  $Re_c = 2 \cdot 10^6$  for LFC airfoils with full chord laminar flow of 14.4 percent and 18.2 percent thickness ratio and the equivalent profile drag contributions of the upper and lower surface. Again, the profile drag increase at higher  $C_L$ 's is relatively small at a given  $Re_c$  value as long as full chord laminar flow can be maintained by means of low drag suction.



Equivalent profile drag  $C_{D\infty}$  (1 of all) laminar LFC airfoils P84 (t/c = .1455) and 182 PJ (t/c = .182),  $Re_c = 2 \cdot 10^6$ ,  $M = .1$ ,  $\theta_{1/4c} = 0^\circ$ , zero losses in section system.

FIGURE 10

The low drag  $C_L$  range with full chord laminar flow with suction depends on the growth of amplified TS-oscillations towards the limits of the low drag  $C_L$  range. The Figure 11 and 12 show for a few typical cases the logarithmic growth factor of amplified TS-waves towards the upper and lower limit of the low drag  $C_L$  range at sailplane Reynolds numbers.

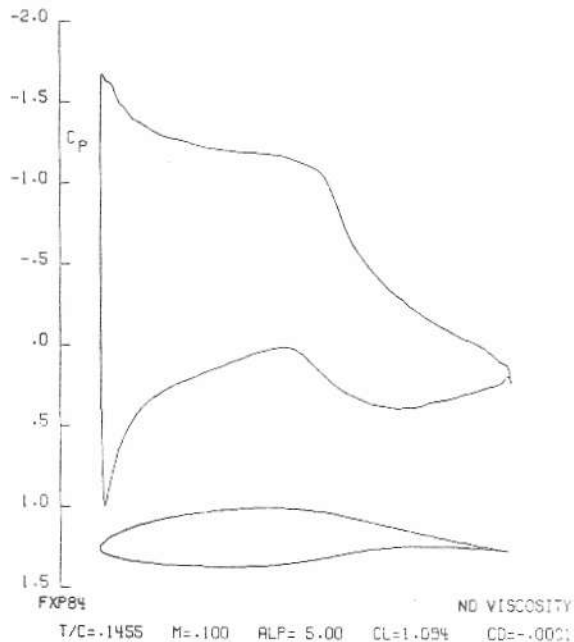


FIGURE 11 A. FXP 84 potential flow chordwise pressure distribution at 5 degree angle of attack.

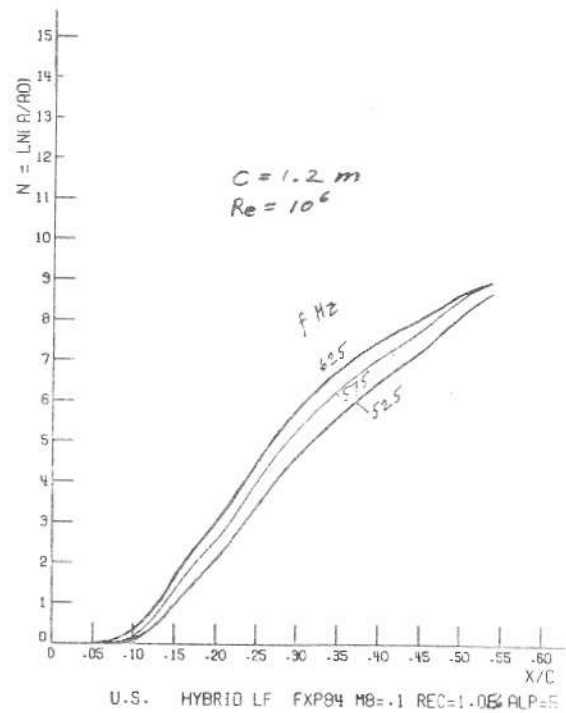


FIGURE 11 B. FXP84 amplification of Tollmien-Schlichting waves at 5 degree angle of attack.

$C^*/4 = -.1033$

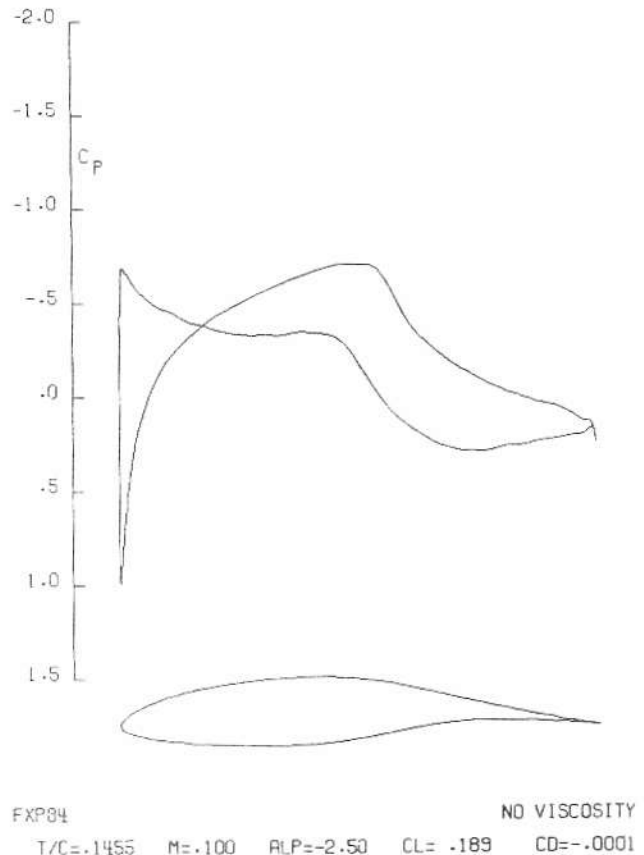


FIGURE 12 A. FXP84 potential flow chordwise pressure distribution at -2.5 degree angle of attack.

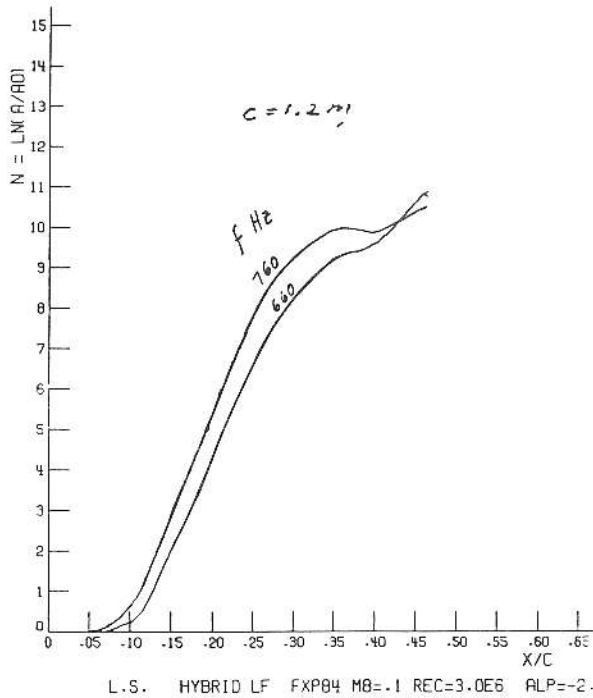


FIGURE 12B. FXP84 amplification of Tollmien-Schlichting waves at 2.5 degree angle of attack,  $Re = 10^6$ .

Figure 13 shows the variation of  $C_{D\infty}$  versus  $Re_c$  up to  $Re_c = 10^7$  for a 14.4 percent thick all laminar LFC airfoil (including  $C_{Dsuction}$  as well as in the suction ducting system, with and without suction drive losses), and a comparison with theoretical values for a 14.3 percent thick natural laminar flow airfoil with transition at  $0.7c$  on both surfaces (according to George Washington University Master's thesis of J. Viken).<sup>13</sup> The equivalent wing profile drag for a fully laminar

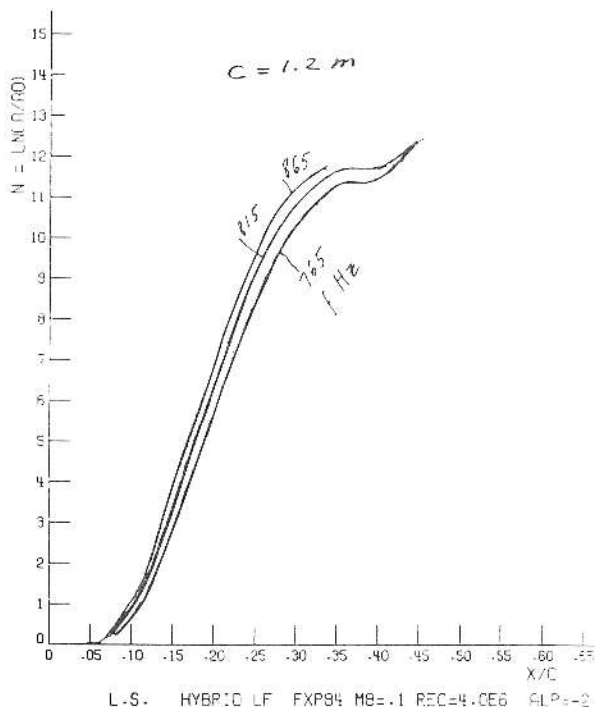


FIGURE 12C. FXP84 amplification of Tollmien-Schlichting waves at 2.5 degree angle of attack,  $Re = 4 \times 10^6$ .

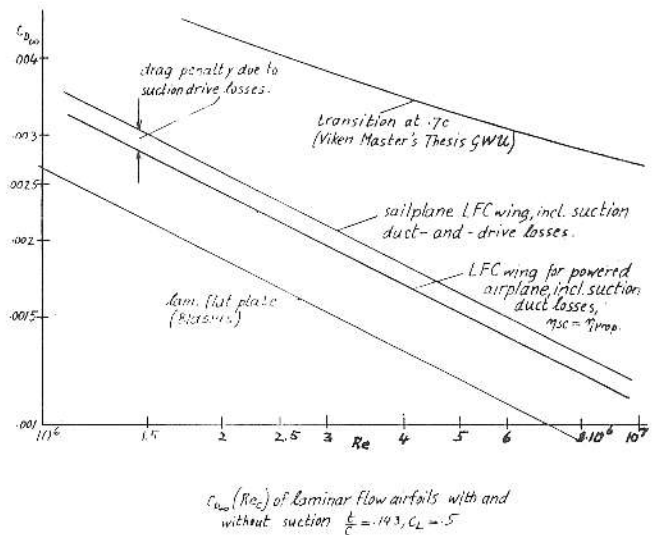


FIGURE 13

LFC wing is substantially smaller than for the natural laminar flow wing, especially at higher  $Re_c$ 's.

Figure 13 shows the equivalent drag penalty due to the suction drive (suction compressor and windmill) losses for  $\eta_{transfer} = .85$ .

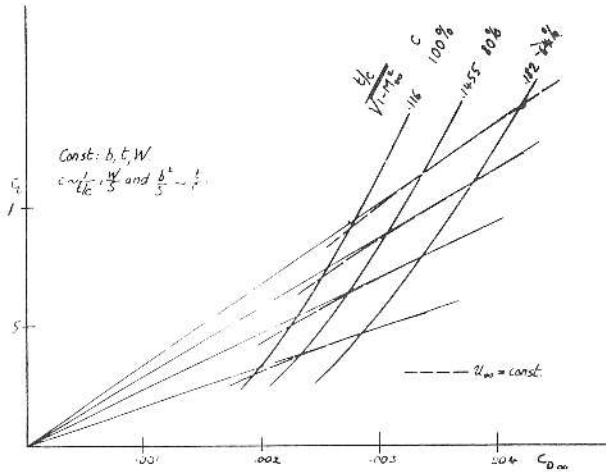
Concerning the choice of wing chord  $c$  and thickness ratio  $t/c$  one might select a wing of larger chord and correspondingly smaller thickness ratio and aspect ratio, operating at lower  $C_L$ 's and higher  $Re_c$ 's with a particularly low  $C_{D\infty}$ , or choose a narrower chord wing with correspondingly larger thickness ratio and aspect ratio, operating at higher  $C_L$ 's (at a given flight speed) and lower  $Re_c$ 's with a correspondingly higher  $C_{D\infty}$  value. It is not immediately obvious whether the larger or smaller chord wing is superior from the standpoint of the section lift to drag ratio  $C_L/C_{D\infty}$  at the same flight speed, especially taking into account the internal suction duct and suction drive losses. For this reason the corresponding profile drag polars  $C_L(C_{D\infty})$  were evaluated for wings of given span  $b$  and constant airplane weight, varying the wing chord and assuming the same absolute wing thickness  $t$  for different wing chords, thereby keeping the structural wing weight for spanwise bending strength constant for different wing chords. The wing chord varies then inversely proportional to  $1/c$  with  $b^2/S$  and  $W/S$  proportional to  $1/c$ .

The results of figures 8-10, and 13, both without and with losses in the suction ducting and suction drive system, were used to evaluate the corresponding profile drag polars (Figures 14a to 16a). Figure 14a neglects losses in the suction ducts and suction drive system. Figure 15a shows  $C_L(C_{D\infty})$  with suction duct losses included but without suction drive losses, corresponding to the case of a powered LFC airplane, with  $\eta_{suction\ compressor} = \eta_{propeller}$ . Suction ducting systems of similar complexity had been assumed for the different wings. Figure 16a includes losses in the suction ducting system as well as in the suction compressor and its drive windmill, corresponding to the case of an LFC sailplane.

Neglecting losses in the suction ducting and drive system (fig. 14a) the optimum LFC airfoil thickness ratio at low  $C_L$ 's and high speeds is relatively large, of the order  $(t/c)_{opt} \cong .18$ , it decreases to 17 percent and 16 percent for

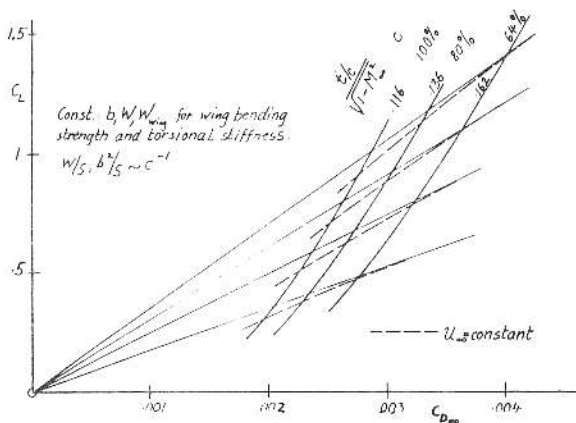
$(L/D)_{\max}$  and  $V_{\text{sink min}}$  respectively, and the optimum chord is surprisingly small.

For similarly complex suction ducting systems with wings of different  $(t/c)$ 's the duct pressure and mixing losses increase rather rapidly with increasing wing thickness ratio, taking into account the larger ratio of  $C_{D \text{ suction}}/C_{D \infty}$  and the higher suction velocities of larger thickness ratio LFC wings due to their lower  $Re_c$ 's and increased rear pressure rise (fig. 15a). In this case, the optimum thickness ratio then varies from  $(t/c)_{\text{opt}} = .145$  at lower  $C_L$ 's and higher speeds to about 0.13 for  $(L/D)_{\max}$  and 0.125 for  $V_{\text{sink min}}$ . Adding, in addition, the losses in the suction compressor and its drive windmill for an LFC sailplane,  $(t/c)_{\text{opt}}$  decreases to values of the order 12 percent (fig. 16a). The corresponding optimum chord increases then accordingly.



All laminar LFC airfoils.  
 $C_{Do}(C_L)$  for various  $t/c$ , no losses in suction ducts and drive.

FIGURE 14 A.

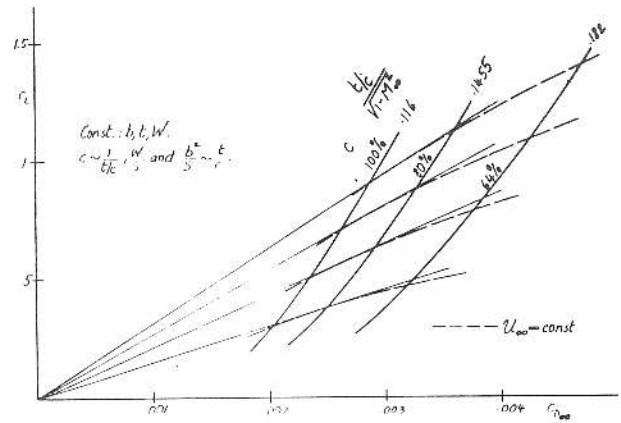


All laminar LFC airfoils.  
 $C_{Do}(C_L)$  for various  $t/c$  and  $c$ . No losses in suction system.

FIGURE 14 B.

If more complex suction ducting systems were acceptable for relatively thicker wings the optimum thickness ratio increases, leading to smaller chord wings.

Of course, these considerations are affected by other secondary factors. For example, wing torsional stiffness is easier



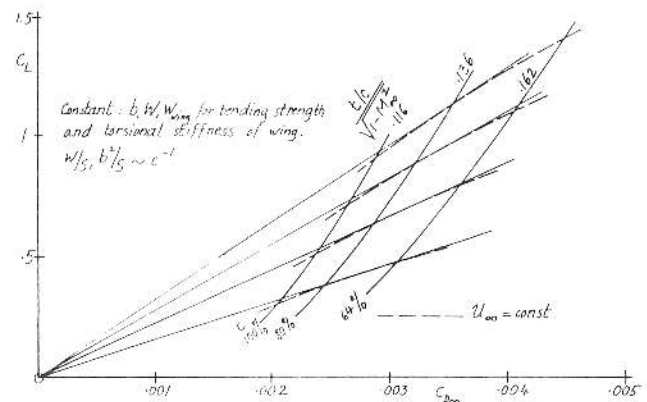
All laminar LFC airfoils.  
 $C_{Do}(C_L)$  for various  $t/c$ , incl. suction ducting losses. Same number of suction ducts.  $\eta_{sc} = \eta_{prop}$ .

FIGURE 15 A.

to control for a smaller chord wing of larger thickness ratio for a given wing span and thickness  $t$ . Assuming the same wing structural weight needed for wing bending strength plus torsional stiffness, the smaller chord wing of larger thickness ratio can be somewhat thinner (smaller  $t$ ) than the larger chord wing of smaller thickness ratio. The corresponding profile drag polars with and without duct- and -drive losses are shown in Figures 14b and 16b. The optimum wing chord is then smaller and the optimum thickness ratio is shifted to higher values, as compared to the case of constant wing thickness  $t$ .

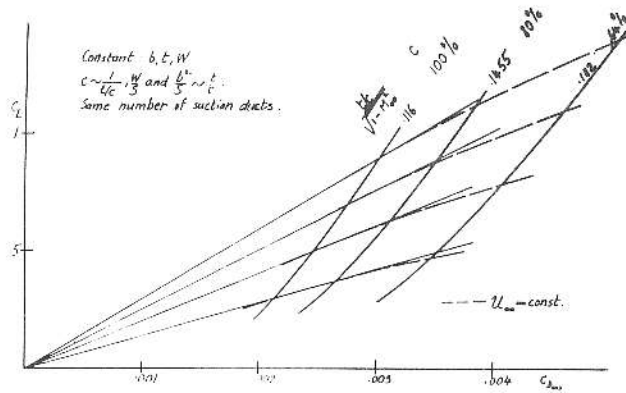
In addition, the induced yawing moment due to roll is smaller with a smaller chord wing and is thus easier to handle with the vertical control surface.

On the other hand, a larger chord wing of the same absolute thickness can carry more water ballast than a smaller chord wing of the same thickness and span. Narrower chord wings eventually require additional suction laminarized water nacelles located in the outer wing, which increase the drag. Admittedly such nacelles are highly effective in lowering the wing bending moment and raising wing flutter speed, thereby enabling further increased wing span. Alternately, if such external water nacelles are available the airplane can be



All laminar LFC airfoils.  
 $C_{Do}(C_L)$  for various  $t/c$  and  $c$ , with suction duct losses. Same number of suction ducts.  $\eta_{sc} = \eta_{prop}$ .

FIGURE 15 B.



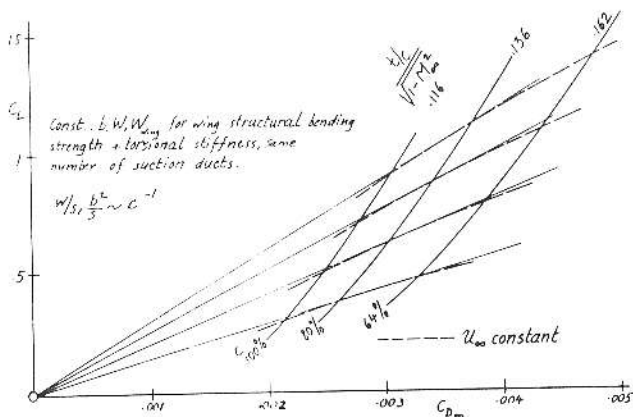
All laminar LFC sailplane airfoils,  $c_{D_{min}}(c_L)$  for various  $(t/c)$ , incl suction ducting and -drive losses ( $\eta_{transm} = .85$ )

FIGURE 16 A.

more heavily overloaded to further improve the high speed performance within safe limits.

Based on all these considerations a 12.8 percent thick all laminar LFC wing of  $\bar{c} = 0.6$  meter average chord and 32.4 meter span was selected, braced externally for structural reasons with suction laminarized wide chord struts of low parasite drag (Figure 17).<sup>14</sup> Externally mounted water nacelles were not considered. The struts alleviate both wing bending as well as torsional moments. Low drag suction is considered to laminarize fuselage, including the junctures between the strut and wing as well as fuselage. With such a relatively thin wing trailing edge cruise flaps will be needed to ensure a satisfactory low drag  $C_L$  range. The rapidly decreasing wing bending moments in the strut-braced inboard part of the wing enable especially thin wing sections in this area with a particularly low profile drag, applying possibly some additional boundary layer suction towards the wing trailing edge to recover part of the kinetic wing wake energy and thus reduce the equivalent drag in this zone still further.

The cantilevered span of this 32.4 meter wing is somewhat larger than the span of the Nimbus 3. Furthermore, its thickness ratio of 0.128 is slightly lower ( $t/c = .14$  for the Nimbus 3); thus the wing structure of the 32.4 meter glider is then correspondingly heavier. Concerning sailplane weight, though, one may perhaps have to rethink: Is it not better to

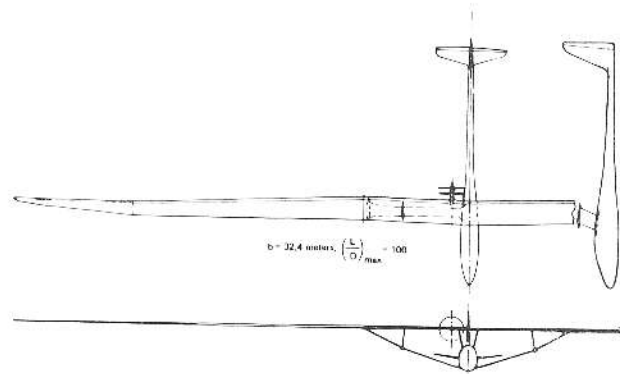


All laminar LFC sailplane airfoils,  $c_{D_{min}}(c_L)$  for various  $t/c$  and  $c$ , with suction duct-and-drive losses ( $\eta_T = .85$ )

FIGURE 16 B.

design the sailplane for less drag with thinner though structurally heavier wings, than filling the wing with water? Admittedly, the thicker and lighter wing will turn tighter without water ballast, but the thinner wing will have a higher  $L/D$  (with and without water ballast). Therefore, it may be a better trade to sacrifice structural weight against improved aerodynamic performance, at least as long as high performance sailplanes will be overloaded with water under good soaring conditions.

Relatively high modulus graphite appears desirable for the wing torsion box and the strut to control wing torsional deformations and strut buckling without excess structural weight, while high strength graphite would be used for the spar caps. Boron is superior in compression and perhaps worthwhile in the compression spar cap in spite of its high price.



All Laminar LFC Sailplane

FIGURE 17

With complete suction laminarization of wing, fuselage, struts and tail surfaces a phenomenal speed polar with  $L/D_{max}$  values approaching 100 appears feasible. In order to be able to utilize the exceptional high speed performance of such an LFC sailplane, especially with water ballast, particular emphasis must be given to raise its flutter speed even at the cost of additional structural weight and balance weight in the wing leading edge. At high speeds, increased attention must be given to avoid aileron reversal, minimize the loss in longitudinal and directional stability and control due to fuselage bending, and avoid excessive wing gust and dynamic loads. One may have to borrow solutions and approaches from high speed powered airplanes, such as alleviation of wing gust and other loads through active control beyond a certain load factor at higher speeds. A small span aileron, located further inboard, may be preferable at high speeds, with the remaining low speed aileron segments locked.

With the large reduction in equivalent wing profile drag by means of low drag suction, the minimization of fuselage drag through suction laminarization becomes important, especially at lower  $C_L$ 's and higher cruising speeds. The fuselage length Reynolds numbers  $Re_L$  of a 30 meter LFC sailplane vary from  $15 \cdot 10^6$  at lower speeds to  $50 \cdot 10^6$  during high speed cruising. These values are lower than those achieved with full length laminar flow on the Reichardt LFC body of revolution, i.e. full length laminar flow and an extremely low fuselage drag should be possible by means of low drag suction, closely approaching area suction. With increasing unit length Reynolds number  $U_{\infty}/\nu$  the fuselage drag coefficient would

then decrease essentially inversely proportional to

$$\sqrt{\frac{U_\infty}{\nu}}$$

Of course, suction laminarization of a wing fuselage juncture presents a formidable challenge, aggravated by the fact that the flow direction in the juncture area changes for different flight conditions, especially in the front stagnation region of the wing. Furthermore, when the trailing edge cruise flap, extending along the entire span towards the fuselage, is deflected, difficulties arise with the suction laminarization of the fuselage in the area downstream of the wing trailing edge. These difficulties can be greatly alleviated or avoided by the compromise solution of mounting the wing above the fuselage on suction laminarized pylon struts, whose junctures with the fuselage are easier to laminarize through suction than the particularly difficult wing-fuselage juncture. At the same time a large vertical distance is thus provided between the wing and strut attachment on the fuselage, structurally desirable for the wing-strut system.

#### D. PERFORMANCE OF A LARGE SPAN ALL LAMINAR LFC SAILPLANE

Figure 17 shows a three-view drawing of such a strut-braced 32.4 meter low drag suction all laminar flow sailplane with the following characteristics:

- span  $b=32.4$  meters
- average chord  $\bar{c}=0.6$  meters
- wing aspect ratio  $b^2/S=54$
- wing area  $S=19.4m^2$
- wing thickness ratio  $t/c=.128$
- wing loading with and without ballast
- $w/s=36$  and  $60$   $kg/m^2$ , respectively

A wing planform somewhat similar to that of an albatross wing was selected (see albatross photo **Figure 18**, taken by the Duke of Edinburgh).<sup>15</sup> Using ideas by W. Schuemann,<sup>16</sup> the outer wing is swept back slightly to move decelerated boundary layer in the rear part of the wing at higher  $c_L$ 's towards the wing tip. Further inboard up to the wing strut intersection region the trailing edge is swept slightly forward to move decelerated boundary layer in the trailing edge region at higher  $c_L$ 's towards the area of the wing-strut intersection, thereby maintaining attached flow in the critical two-third half span region at high lift close to the stall. The inboard strut-braced part of the wing would be swept back slightly to generate a spanwise boundary layer flow away from the fuselage to avoid premature wing stall in the area upstream of the tail surfaces.

A full-span small chord trailing edge cruise flap raises the low drag  $c_L$  range and is used for aileron control at lower speeds, assuming full chord laminar flow through suction for smaller flap deflections. At very high speeds a short span aileron provides lateral control, with the remaining flap surfaces locked in place.

The performance of similar LFC sailplanes was analyzed for sea level conditions both with and without water ballast, using results from a boundary layer analysis on the wing to evaluate the equivalent wing profile drag  $C_{D\infty}$  and suction



*Albatross in Flight*

FIGURE 18

drag  $C_{D\text{ suction}}$  adding suction ducting and mixing losses as well as suction compressor and drive windmill losses (transfer efficiency 85 percent, optimum suction air exhaust velocity 85 percent of flight speed). Results from the Reichardt LFC body of revolution were used to estimate the equivalent drag of the fully suction laminarized fuselage.

**Figure 19** shows the drag polars  $C_L(C_D)$  of a 30 m LFC sailplane with  $t/c=.117$  for the wing with and without water ballast, as well as of the wing along with ballast. The drag polars show a best glide ratio  $(L/D)_{\max}=98.5$  and  $91.4$  with and without water ballast, respectively, at relatively low  $C_L$  values (0.7), considering the high wing aspect ratio of 50.

The corresponding speed polars  $V_{\text{sink}}(U_\infty)$  and glide ratio  $L/D$  versus  $U_\infty$  are shown in **Figure 20** with and without water ballast.

Performance at  $H=0$

$$(L/D)_{\max}$$

$$V_{\text{sink, min}}$$

$$V_{\text{sink}} \text{ at } L/D=60$$

$$V_{\text{sink}} = 2m/secat$$

With Ballast

$$98.5 \text{ at } U_\infty = 38.7m/s$$

$$0.33m/s \text{ at } U_\infty = 27m/s$$

$$1.24m/s \text{ at } U_\infty = 74.4m/s$$

$$U_\infty = 91m/s, L/D=46$$

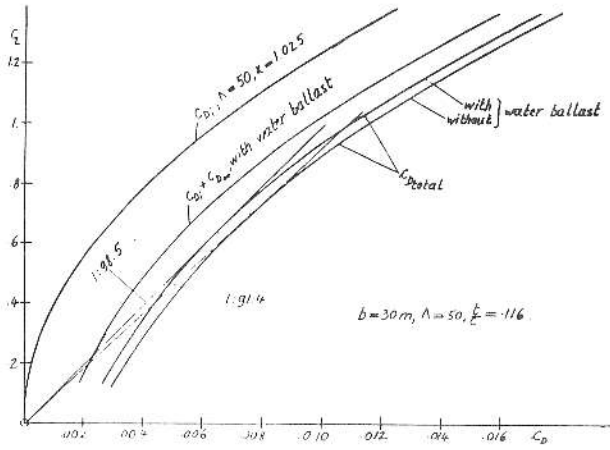


FIGURE 19 All laminar single seater LFC sailplane,  $C_L$  ( $C_D$ )

Without Ballast

91.4 at  $U_\infty = 29\text{m/s}$

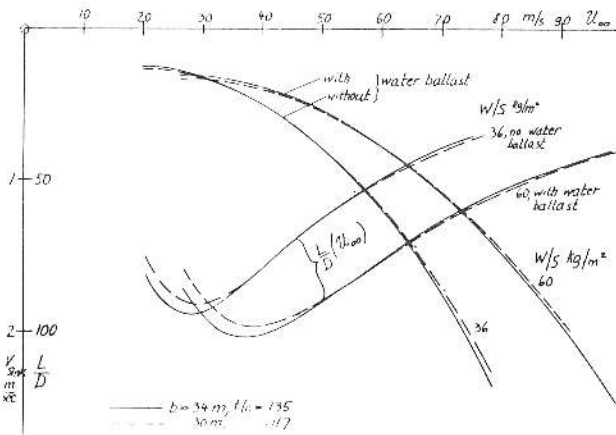
0.27m/s at  $U_\infty = 21\text{m/s}$

0.88m/s at  $U_\infty = 52.2\text{m/s}$

$U_\infty = 74.3\text{m/s}$ ,  $L/D = 37.5$

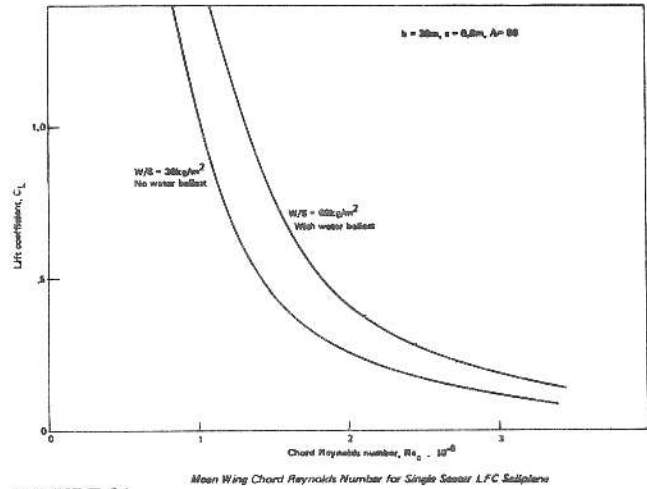
The lower length Reynolds numbers without water ballast (see variation of  $Re_c$  with  $C_L$ , Figure 21) increase  $C_{D\infty}$  and  $C_{D\text{parasite}}$  to lower accordingly  $L/D$  over the corresponding values of the ballasted sailplane. A similar performance degradation occurs at higher flight altitudes.

Figure 20 shows for comparison the speed polar  $v_{\text{sink}}(U_\infty)$  and  $L/D(U_\infty)$  of a 34 meter LFC sailplane with a 13.5 percent thick wing of 0.6 meter mean chord (with and without ballast). It has a lower  $v_{\text{sink min}}$  and higher  $(L/D)_{\text{max}} = 102$ ; the high speed performance, on the other hand, is slightly better for the 30 meter sailplane due to its thinner wing.



Single seater LFC sailplane,  $\frac{L}{D}(U_\infty)$ ,  $v_{\text{sink}}(U_\infty)$

FIGURE 20

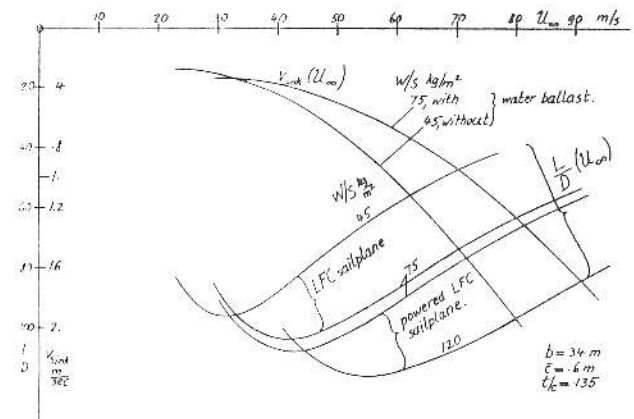


Mean Wing Chord Reynolds Number for Single Seater LFC Sailplane

FIGURE 21

Figure 22 shows the speed polars and  $L/D(U_\infty)$  for the same 34 meter sailplane, modified as a two-seater with a fully suction laminarized fuselage. With the higher wing loading of this two-seater and the correspondingly higher flight speeds and Reynolds numbers the resulting reduction in  $C_{D\infty}$  more than compensates for the larger fuselage drag to raise accordingly  $L/D$  slightly over the corresponding values of the 34 meter single seater (fig. 22)  $\{(L/D)_{\text{max}} = 103.6\}$  with water ballast. If this two-seater were powered and propelled by a propeller, with its efficiency equal to that of the suction compressor, one would not have to account for the aerodynamic losses in the suction compressors and their drive windmill as in the LFC sailplane, raising  $L/D$  accordingly further (fig. 22). Still higher  $(L/D)$  could, in principle, be possible with such a powered LFC two-seater at further increased wing loadings.

One might consider driving the suction compressors of an LFC sailplane with solar energy using solar cells. The question arises whether or not a solar powered airplane will still be considered a sailplane. Solar energy might then be applied just as well to sailplanes without low drag suction. The author has, therefore, not considered the use of solar cells to drive the suction compressors.



2-Seater LFC sailplane and powered LFC sailplane Performance

FIGURE 22

After discussing the overall design and the performance of large span all laminar LFC sailplanes with low drag suction the important question arises as to how to design and build such an LFC sailplane. Many new and unconventional detail problems and questions arise in the design of such a low drag suction sailplane, which are not encountered in conventional high performance sailplanes. The following chapters try to present solutions to some of these problems and questions.

## E. DETAIL DESIGN CONSIDERATIONS

### 1. Influence of suction ducting considerations on the choice of the airfoil sections

The choice of the airfoil section is decisively influenced by suction ducting design considerations. These are particularly critical for an LFC sailplane in view of the large wing aspect ratio and the relatively high nondimensional suction volume rates  $C_Q$  at the low wing chord Reynolds number of an LFC sailplane, as seen from the following analysis of the suction volume rates.

For a LFC sailplane wing, operating at low  $Re_c$ 's and in the absence of any significant boundary layer crossflow the equivalent area suction velocity  $v_0$  needed to maintain laminar boundary layer profiles of the Blasius type

$$\left( \frac{\partial^2 u}{\partial y^2} = 0 \text{ at the wall } y = 0 \right)$$

through the rear pressure rise of the upper and lower surface, can be evaluated to a satisfactory first approximation from the boundary condition at the wall  $y=0$  for the x-boundary layer momentum equation with

$$v_0 \left( \frac{\partial u}{\partial y} \right)_0 = - \frac{1}{\rho} \frac{\partial p}{\partial x}$$

for incompressible flow. With

$$\frac{\tau_0}{\frac{\rho}{2} U^2} = \frac{0.664}{\sqrt{N}}$$

where

$$N = \frac{1}{3} Re_{\delta_*}^2, \quad Re_{\delta_*} = 2.59 Re_{\theta}$$

and

$$\tau_0 = \mu \left( \frac{\partial u}{\partial y} \right)_0 : \frac{v_0}{U_{\infty}} = -2.25$$

$$\frac{\partial C_p / \partial \left( \frac{s}{c} \right)}{1 - C_p} \frac{Re_{\theta}}{Re_c}$$

Thus, the equivalent area suction velocity ratio  $v_{0\infty}$  is proportional to the chordwise pressure gradient

$$\frac{\partial C_p}{\partial \left( \frac{s}{c} \right)}$$

and inversely proportional to  $(1 - c_p)$  i.e. particularly high suction velocities are needed in strongly decelerated flows and at high static pressures with low boundary layer edge velocities  $U_E$ .

Furthermore,  $v_{0\infty}$  is proportional to  $Re_{\theta}$  in the pressure rise area and inversely proportional to  $Re_c$ . Since

$$Re_{\theta} \sim \sqrt{Re_c}, \quad \frac{v_0}{U_{\infty}} \sim \frac{1}{\sqrt{Re_c}}$$

$$\text{or } \frac{v_0}{U_{\infty}} \sqrt{Re_c} = v_0^* = \text{constant}$$

constant, i.e., the same percentage of the boundary layer is removed by suction at different  $Re_c$ 's. (In practice, somewhat smaller  $v_0$ -values with correspondingly less stable boundary layer profiles are permissible at lower  $Re_c$ 's and vice versa.)

Of course,  $Re_{\theta}$  is not known a priori in the rear pressure rise area. For pressure rises with moderately large adverse pressure gradients, example calculations have shown that  $Re_{\theta}$  stays approximately constant through the rear pressure rise and is close to the value at the start of the pressure rise, which can be obtained from a boundary layer analysis in the area upstream of the rear pressure rise. Using then  $Re_{\theta}$  at the beginning of the pressure rise furnishes immediately a surprisingly good first approximation for the area suction velocity  $v_0$  which is needed to maintain a reasonably stable laminar boundary layer in this region. It can be further iterated if necessary.

For a very steep rear pressure rise  $Re_{\theta}$  decreases slowly with increasing static pressure. This can be verified by decelerating the boundary layer infinitely rapidly, using Bernoulli and conservation of mass to construct the decelerated new boundary layer profiles, removing the innermost slowest boundary layer particles, as they are continuously decelerated to zero velocity at the wall in the pressure rise zone.

For a rear pressure rise which is less steep surface friction  $\tau_0$  will add to the boundary layer momentum deficiency and thus lead to a nearly constant  $Re_{\theta}$  in the pressure rise area. When the pressure rises relatively slowly the contribution of  $\tau_0$  to  $Re_{\theta}$  is correspondingly larger and  $Re_{\theta}$  then grows slowly as the static pressure increases through the rear pressure rise zone.

Thus, this analysis is highly satisfactory for reasonably steep rear pressure rises up to modest wing chord Reynolds numbers, as long as TS-waves are not excessively amplified and boundary layer crossflow disturbance vortices are absent. For very steep or flat pressure rises iterations will usually be needed to establish the optimum suction rates needed for suction laminarization.

According to this analysis the local and overall suction flow rates of LFC wings vary approximately proportional to the pressure gradient

$$\frac{\partial C_p}{\partial \left( \frac{s}{c} \right)}$$

which is proportional to the airfoil thickness ratio  $1/c$ .  $1 - c_p$ , though, is somewhat larger for thicker airfoils, as compared to thinner ones, to compensate somewhat for the influence of their larger pressure gradients in estimating the required suction velocity ratio in the rear pressure rise area. Since a small percentage of the rear pressure rise towards the wing trailing edge can be accomplished without suction with natural laminar flow, the assumption that the suction flow rates increase nearly proportional to  $1/c$  is reasonably well justified.

The suction duct total pressure drop

$$\frac{\Delta p}{\frac{\rho}{2} U_{\infty}^2} = \Delta c_{pD}$$

can then be expressed for LFC wings of different wing chords and wing aspect ratios  $\Lambda_d$  per duct length for wings of a given

thickness  $t$ , assuming that the nondimensional suction flow coefficient

$$C_Q \sim \frac{t}{c \sqrt{Re_c}}$$

(See previous remark concerning the variation of  $C_Q$  with  $Re_c$ ). The following result follows then for the suction duct total pressure drop coefficient.

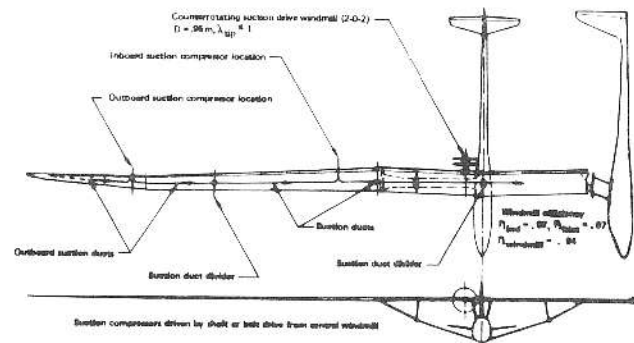
$$\Delta C_{pDuct} \sim \frac{\Lambda d^3}{U_\infty \sqrt{c.t}}, \text{ i.e. } \Delta C_{pDuct} \sim \Lambda d^3$$

$$\sim \frac{1}{U_\infty/\nu} \text{ and } \frac{1}{\sqrt{c.t}}$$

Thus, the wing suction ducting design is particularly difficult for large wing aspect ratios  $\Lambda_d$ , per duct length, especially for sailplanes in view of their small chord  $c$  and absolute wing thickness  $t$ . In this respect the suction ducting problems of the wing of a much larger powered LFC airplane are much easier to cope with in view of their larger wing chord  $c$  and thickness  $t$ . On the other hand, a relatively large percentage of the wing volume behind the spar can be used in a LFC sailplane for suction ducting, in contrast to the wet wing of a powered LFC airplane, which often carries additional fuel in the space behind the spar.

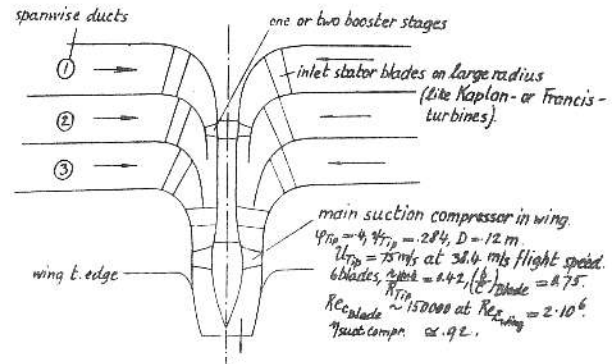
Since, (for the same wing span and thickness  $t$ ) the wing aspect ratios  $I = b^2/s$  and  $I_d$  (for the same number of spanwise ducts) are proportional to  $1/c$  the suction ducting design of LFC sailplane wings is particularly difficult for LFC wings of larger thickness ratios. Vice versa the suction ducting problems are greatly alleviated with LFC wings of smaller thickness ratios  $1/c$  and correspondingly lower aspect ratios.

These suction ducting considerations have decisively influenced the choice of a relatively small airfoil thickness ratio. Even so, to minimize the suction duct pressure losses and thereby alleviate, at the same time, the problems in achieving the correct spanwise suction distribution, it will be necessary to subdivide the spanwise ducts of each wing side into three and probably four spanwise ducts, feeding into two axial flow suction compressors, with their axis aligned in flight direction and driven by one or several windmills (Figure 23). Relatively thicker wings of higher aspect ratio would require a still more elaborate subdivision of the spanwise ducts to keep the duct pressure losses within bounds.



Subdivision of Suction Ducts Along Wing Span to Minimize Duct Losses and Ensure Proper Spanwise Suction Distribution

FIGURE 23 A.

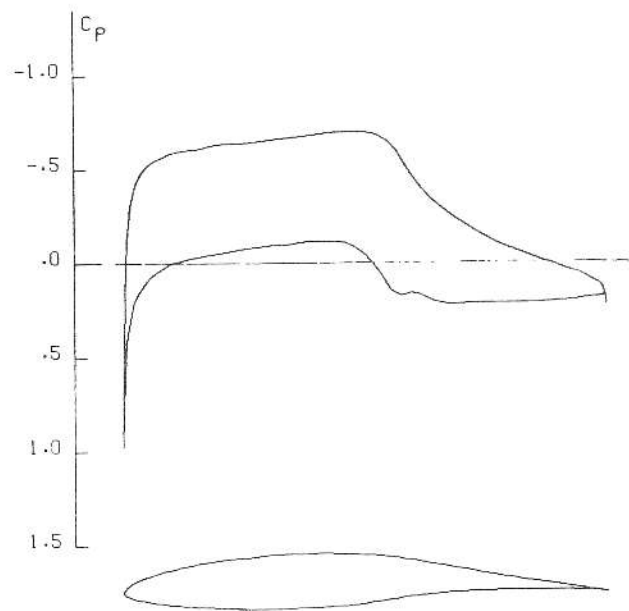


Suction air collector, schematic.

FIGURE 23 B

The reduction of duct pressure drop losses is not necessarily as important from the standpoint of performance; what is rather more important is to ensure the correct suction inflow distribution along the span, which depends on the pressure difference between the external surface and the duct. Errors in these suction rates can be kept lower with smaller duct pressure losses. For this reason, it is critically important to carefully study the suction ducting design problems of a large span LFC sailplane and minimize the duct pressure drop- and mixing losses in the suction ducting system.

The question now arises concerning the design of suitable LFC airfoils with chordwise pressure distributions which alleviate the suction ducting design. The following approach is shown in the airfoil P84R, whose contour and pressure distribution is shown in Figure 24. The pressure rise starts relatively far upstream at around 53 percent chord on the upper surface and somewhat further upstream on the lower surface



P84R INVISCID  
M=1.00 ALP=1.000 CL=.483 CMC/4=-.0814 T/C=.117

FIGURE 24. P84R potential flow chordwise pressure distribution.

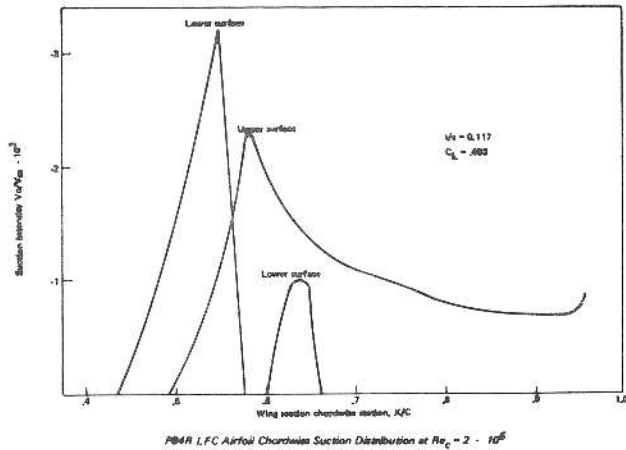
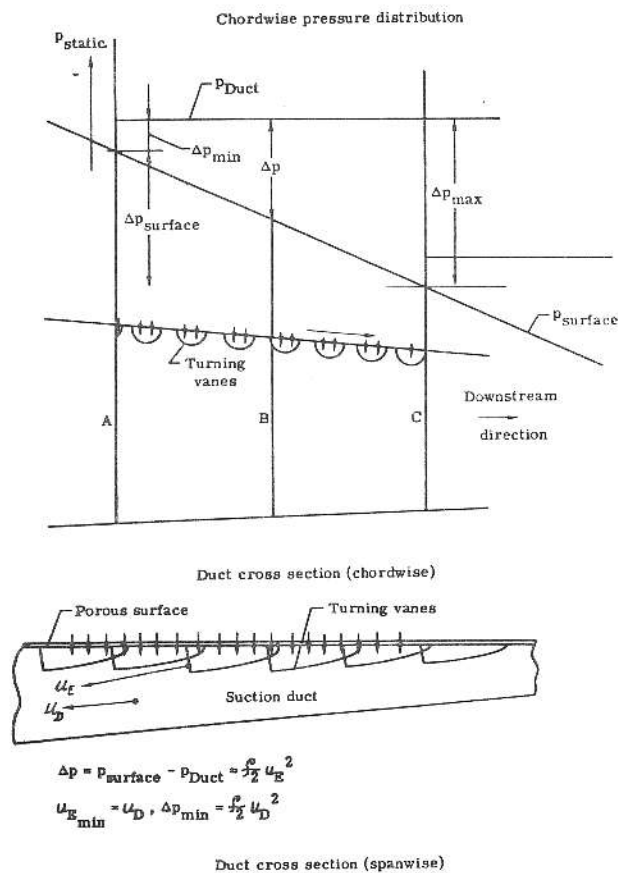


FIGURE 25.

and is strongly concave, with the steepest pressure rise occurring close to the location of minimum pressure and decreasing continuously in downstream direction. As a result, the equivalent area suction velocities (Figure 25) are highest around 50 percent to 60 percent chord, where the airfoil is still sufficiently thick, thereby providing adequate cross sectional area for the spanwise suction ducts. The suction air can then be turned directly into the spanwise suction ducts through small turning vanes without using additional chordwise ducting (Figure 26). The pressure rise on the lower surface is staggered 5 percent upstream with respect to that of



Suction air mixing method (b) in rear pressure rise area of LFC wings.

FIGURE 26

the upper surface to provide suction and suction duct space upstream of the suction ducts for the upper surface. A large part of the airfoil cross sectional area downstream of the spar can then be used for suction ducting, with the chordwise external pressure distribution tailored for the specific needs of the suction ducting design without the use of additional chordwise ducting.

Advantages of LFC airfoils with a relatively early concave rear pressure rise are a larger low drag  $C_{L}$ -range, as compared to LFC airfoils with the rear pressure rise located further downstream. Figure 27 shows the variation of the low drag  $C_{L}$ -range for LFC airfoils of different thickness ratios  $t/c$  and chordwise location  $\bar{x}$  for the start of the rear pressure rise  $\bar{x} =$  average location between upper and lower surface), as analyzed from Korn-Garabedian analysis calculations of LFC airfoils of different  $t/c$  and  $\bar{x}/c$  values. The low drag  $C_{L}$ -range varies proportional to  $(t/c)^{1.50}$  and increases with a more forward location for the start of the rear pressure rise. The equivalent wing profile drag  $C_{D0}$  of all laminar LFC airfoils decreases slightly when the rear pressure rise starts further downstream (fig. 8, 9). Since this drag variation with  $\bar{x}/c$  is not too significant the designer has more possibilities to judiciously select the airfoils of LFC sailplanes at various spanwise stations from the standpoint of aerodynamic performance, roll control, roll damping, low drag  $C_{L}$ -range, etc., as long as full chord laminar flow can be maintained through suction for different chordwise pressure distributions.

From the standpoint of equivalent profile drag LFC airfoils with a more downstream location of the rear pressure rise are slightly superior. The Figures 28a and 28b show results of a boundary layer analysis with area suction and full chord laminar flow for J. Viken's 14.3 percent thick airfoil (from his George Washington University Master's Thesis<sup>13</sup>)

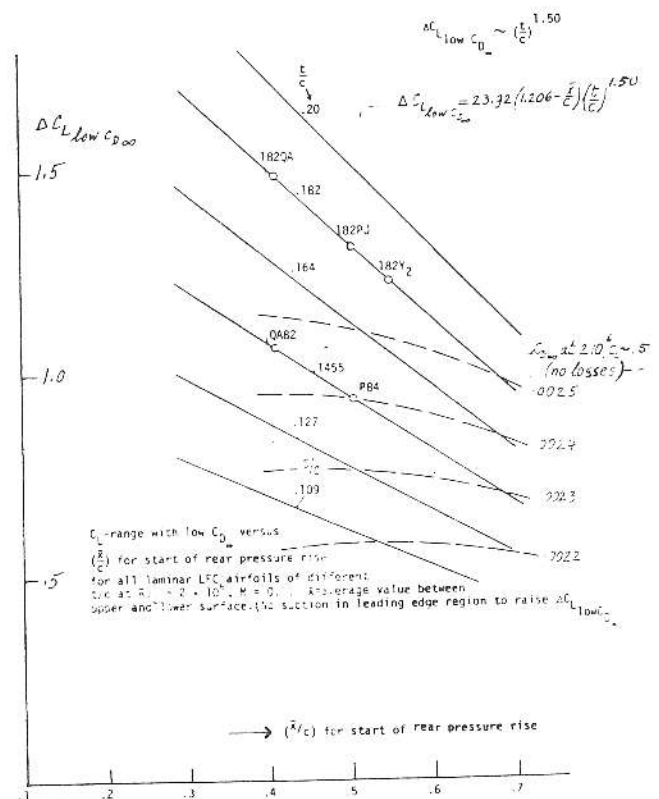


FIGURE 27. Suction airfoil  $C_L$ -range with low drag, no losses.

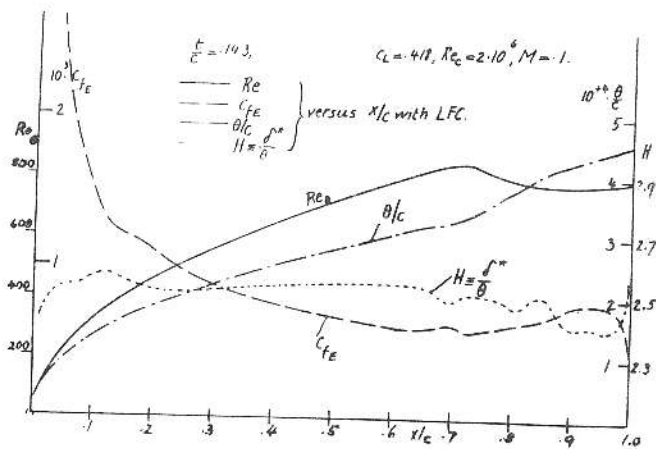


FIGURE 28 A. NLF upper surface computed boundary layer characteristics.

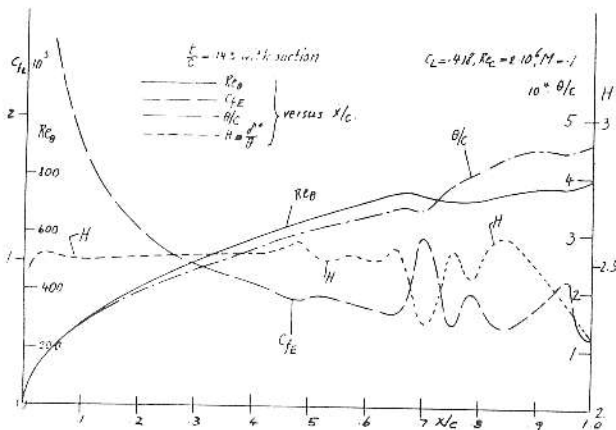
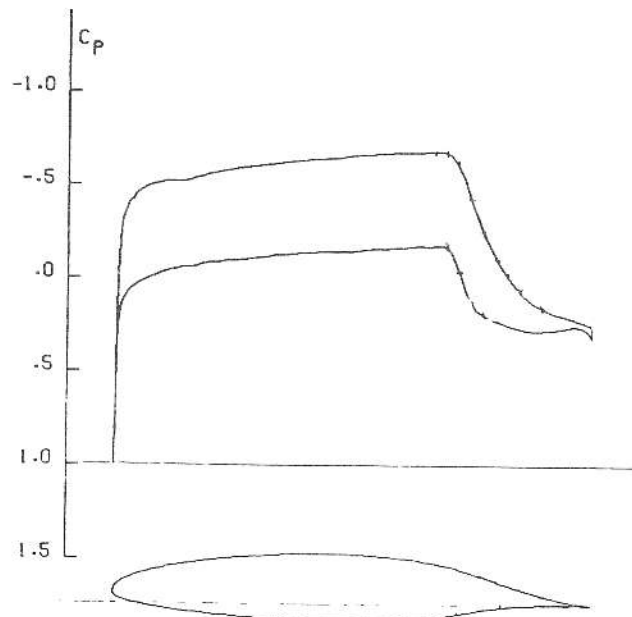


FIGURE 28 B. NLF lower surface computed boundary layer characteristics.

at  $c_L = .42$  and  $Re_c = 2.10^6$ . The corresponding pressure distribution and contour are shown in Figure 29. The rear pressure rise starts on both surfaces at  $0.70c$ . The corresponding chordwise distribution of suction velocity and suction power is presented in Figures 30a and 30b, showing suction within the narrow zone of the steep rear pressure rise with correspondingly high area suction velocities.

With such a rearward location  $x/c$  for the start of the rear pressure rise the low drag  $c_L$ -range, of course, decreases for a given  $V/c$ -ratio. However, plotting the low drag  $c_L$ -range versus  $x/c$  for LFC airfoils of constant equivalent profile drag  $C_{D\infty}$ ,  $V/c$  increases somewhat with increasing  $x/c$ . Thus, the low-drag  $c_L$ -range for constant  $C_{D\infty}$ -values decreases at a slower rate with  $x/c$ , as compared to the case when  $V/c$  is held constant, both for the cases with and without losses in the suction ducting and drive system (Figure 27 and Figures 31, 32). Furthermore, with such an aft location of the rear pressure rise the airfoil will be thicker in the area towards the trailing edge. It is then somewhat easier to design a small chord trailing edge cruise flap with a concave "corner" at the flap hinge on the upper surface. The flap down deflections may then be increased, thereby raising the low drag  $c_L$ -range due to flap deflection to compensate for the loss in low  $c_L$ -range at a given flap setting.

When suction is concentrated rather far downstream on the airfoil ( $x/c = .7$ ), the suction air of the upper surface must then be ducted upstream, for example, through chordwise corrugations, etc., into the main spanwise suction ducts.



NLF (1) -0414F INVISCID  
 $M = .100$   $ALP = -.953$   $CL = .418$   $CNC/C = -.0790$   $T/C = .143$

FIGURE 29. NLF chordwise pressure distribution.

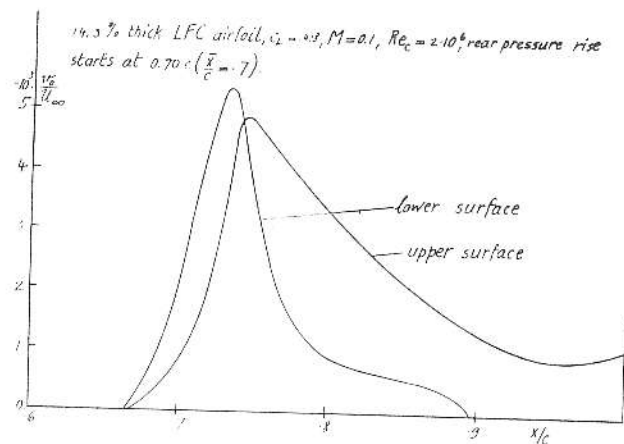


FIGURE 30 A.

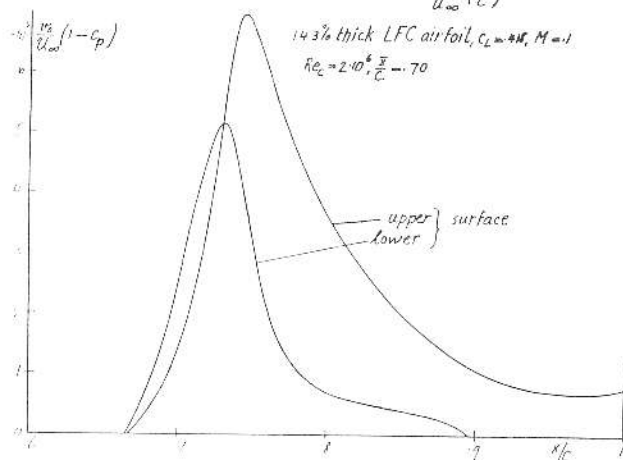


FIGURE 30 B.

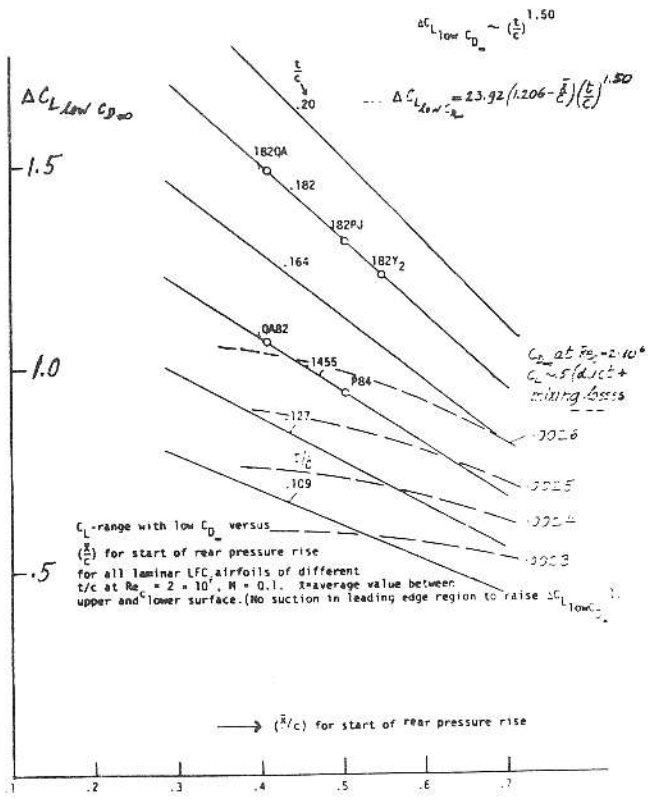


FIGURE 31. Suction airfoil  $C_L$ -range with low drag; duct and mixing losses included.

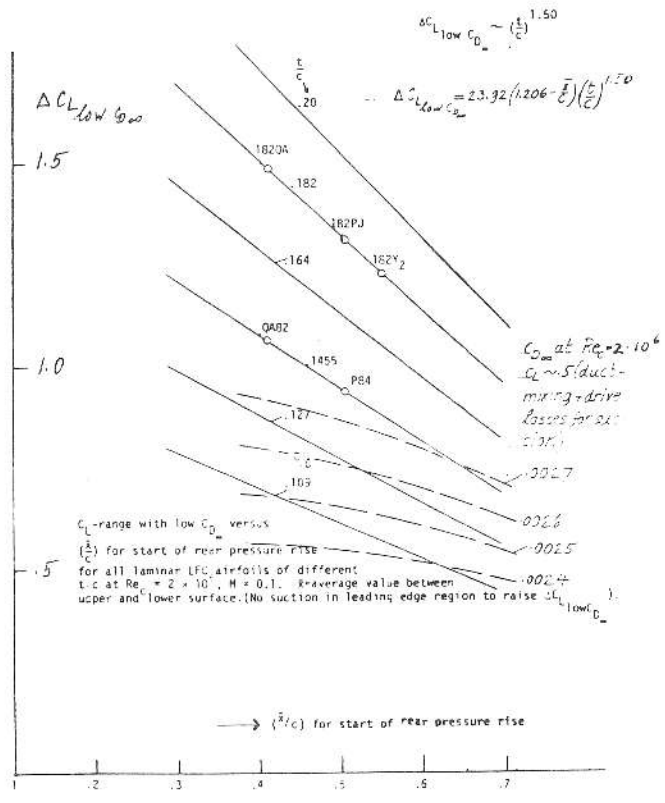
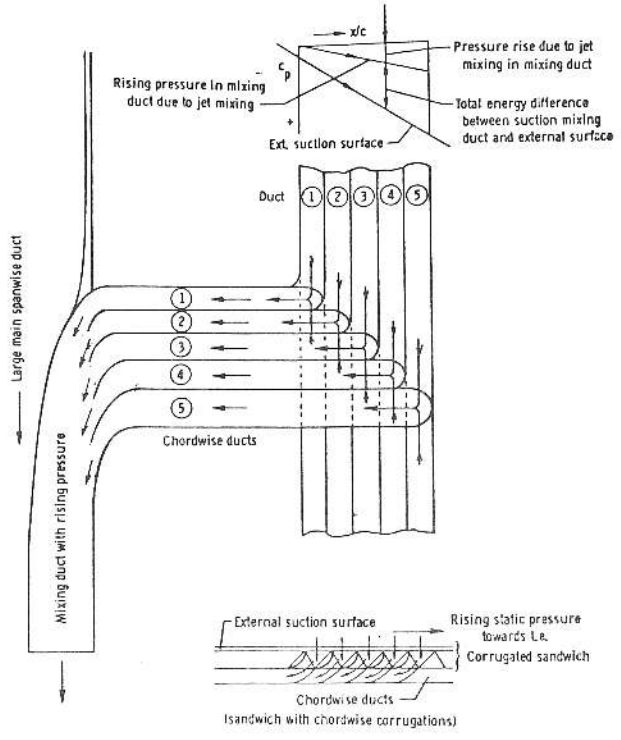


FIGURE 32. Suction airfoil  $C_L$ -range with low drag, duct mixing and pumping losses included.

There are located further upstream in an area where adequate cross sectional area is available (Figure 33 a-c). This solution is, no doubt, more complex; it allows, however, a more efficient jet mixing of the suction air of different total pressure in the pressure rise zone (see next chapter) to either decrease the suction air mixing losses in the rear pressure rise area, or alternatively reduce the number of individual spanwise ducts for a given sum of duct pressure and mixing losses. Alternately, with the same number of ducts and duct losses one might increase the wing thickness ratio and wing span and thereby further raise  $(L/D)_{max}$  and reduce  $v_{sink min}$ . These duct considerations are discussed in the next section.



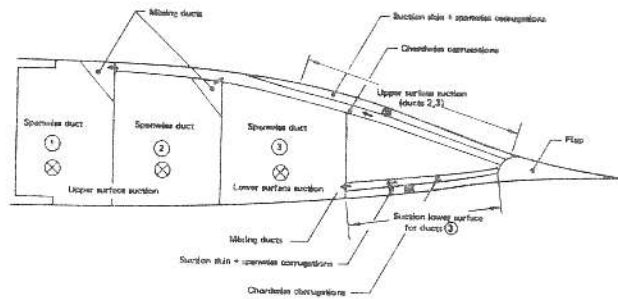
Schematic suction ducting system in rear pressure rise area of LFC wing with duct mixing method b.

FIGURE 33 A.

**II. General Basic Considerations of LFC Suction Ducting Layouts and Losses** (see for example reference 17)

The total energy losses in the suction ducting system of LFC wings between the external surface and the suction compressor consist of kinetic energy-, throttling- and mixing losses, as well as flow separation-, duct wall friction- and secondary flow losses. Which one of these losses dominates depends on the type of suction ducting design, the suction method selected and to a large extent on the aerodynamic refinements applied in the ducting design.

The aerodynamically ideal LFC area suction is assumed to be closely approached by suction either through a large number of closely spaced spanwise slots, perforated surfaces with a very large number of small holes or a porous surface. In a similar manner as the blood in the human body is carried from a large number of capillaries to progressively larger and fewer blood vessels and finally to the heart, the suction air passes through small openings in the external LFC surfaces



Suction Ducting Layout in Wing (Schematic) GLBE Airfoil

FIGURE 33 B.

at low velocities and flow Reynolds numbers. It is then ducted to progressively larger and fewer suction ducts at increasingly higher duct flow velocities and Reynolds numbers and finally to the suction compressors. Thus, due to the very low flow Reynolds numbers in the external suction skin viscous friction losses dominate there, while kinetic energy exit losses at the downstream side of the suction skin are usually less important in view of the low velocities involved, when area suction is closely approached. The dominating viscous flow forces in the external suction skin suppress the formation of turbulent eddies at the low flow Reynolds numbers involved to allow aerodynamically relatively crude flow passages in this skin (Figure 34).

After passing through the suction skin the suction air is collected in small spanwise plenum chambers, located underneath the external suction skin, which serves to maintain a sufficiently uniform spanwise suction distribution. From

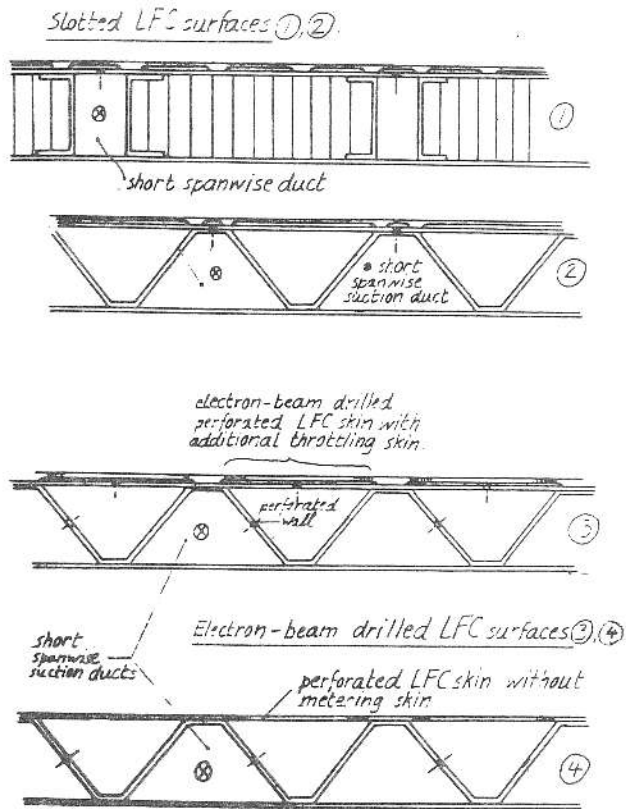


FIGURE 34 Section surface construction.

these plenum chambers the suction air is ducted through holes, drilled in a continuous structural inner skin, into relatively small first spanwise suction ducts formed, for example, by the structural elements of a corrugated sandwich skin. To retain most of the spanwise momentum of the suction air during its passage from these holes into these first spanwise ducts and at the same time minimize duct losses, the above mentioned holes may be drilled at an oblique angle to the skin; furthermore, stress concentrations around these holes in the structurally particularly critical spanwise direction under the action of vertical bending loads would be substantially reduced to greatly improve the fatigue life of the inner skin. Low duct flow velocities in the first spanwise ducts are easily possible and enable small duct losses even with a relatively crude introduction of the suction air into these ducts through perpendicular or oblique holes.

Since the above mentioned sandwich skin and the rear part of the wing are often too thin to carry the suction air over long spanwise distances in such first spanwise ducts in a corrugated sandwich skin, the suction air must then be ducted from these first spanwise ducts within relatively short intervals to short chordwise ducts, whenever the rear pressure rise and suction are located relatively far downstream. These chordwise ducts dump the suction air into larger main spanwise ducts, which carry it to the suction compressor. To minimize structural weight these chordwise ducts may be integrated with chordwise ribs, especially in the area of the main load carrying box; in the rear pressure rise area they may be formed by chordwise corrugations integrated for example with a sandwich wing skin and contributing to wing torsional stiffness. The main spanwise ducts can be located in areas where the wing is sufficiently thick to allow long spanwise ducts of adequate cross section and correspondingly small total energy losses, with their vertical walls (lightweight sandwich skins) carrying bending and torsional shear, thus contributing structurally to the wing structure.

One or several suction compressor booster stages may be needed to raise the total pressure of the low pressure ducts to a common total pressure level, from where the suction air is accelerated in the main suction compressor to optimum exhaust velocity in flight direction.

Wherever the suction air is transferred and turned into other ducts at reasonably high local flow Reynolds numbers, flow turning nozzles should preferably be provided to minimize local losses and flow pulsations; local flow separation in these nozzles be avoided and aerodynamic nozzle losses minimized by means of a careful aerodynamic design, providing an adequate overall flow acceleration through them. To retain the momentum of the suction air in duct flow direction and minimize at the same time duct losses the suction air should be introduced into the suction ducts through carefully laid out flow turning nozzles or vanes, preferably in such a manner that secondary flow losses and the relatively high duct friction losses associated with secondary flow in ducts (see for example experience by G. I. Taylor or J. Ackeret) are minimized.

Duct wall friction losses, of course, decrease rapidly by lowering the duct flow velocities, accomplished by increasing the duct diameters and cross-sectional areas, and reducing the duct length to hydraulic diameter ratio  $l/d_{hyd}$ .

### III. Mixing Losses in the Suction Ducting System of the Rear Pressure Rise Zone

The external static pressure and as a result the total pressure of the sucked boundary layer increases substantially from the location of minimum pressure towards the trailing edge of LFC wings, causing additional throttling and/or

mixing losses as a result of the chordwise variation of the pressure difference  $\Delta p$  between the external surface and the suction duct. The question then arises concerning the minimization of the sum of these additional throttling and/or mixing losses and the duct wall friction and secondary flow losses.

The additional duct throttling and/or mixing losses associated with the chordwise variation of the static pressure in the rear pressure rise area of LFC wings can, in principle, be minimized by closely approaching the ideal individual reenergization of each sucked boundary layer particle in a large number of separate relatively small suction ducts with individual suction compressor booster stages, at the cost, of increased complexity and duct wall friction losses (due to larger total duct wetted area with a larger number of ducts). Therefore, to decrease the number of suction ducts in the rear pressure rise area of LFC wings without excessive additional losses the mixing losses of each individual duct should be minimized as follows:<sup>17,18</sup> Instead of throttling the suction air in the outer suction skin and/or the inner structural skin (method a) in slots, holes or other throttling devices, the sucked boundary layer can be injected tangentially (in duct flow direction) into the ducts through flow turning nozzles or vanes (method b) (fig. 29)<sup>17,18</sup>. The pressure drop between the external surface and the duct and thus across the above mentioned flow turning nozzles is largest at the location of the highest external static pressure in the rear part of a particular duct. As a result, the corresponding local nozzle exit flow velocity at the entrance into the duct is a maximum; it is usually substantially larger than the mean duct flow velocity at the same spanwise station. The duct total pressure then rises due to jet mixing according to conservation of mass and momentum to often more than compensate for duct wall friction losses. The corresponding jet mixing efficiency  $\eta_{\text{mixing}}$  is shown in Figure 35. To maintain uniform spanwise suction in the presence of a rising duct total pressure under the action of such jet mixing the duct regions of lower static pressure at the beginning of the duct might preferably be connected with external suction surfaces which are located somewhat further upstream on the wing surface in a region of lower static pressure, and vice versa, thus ensuring reasonably uniform total pressure difference between the duct and the external surface along the span and thereby alleviating the problem of maintaining the correct suction rates along the span.

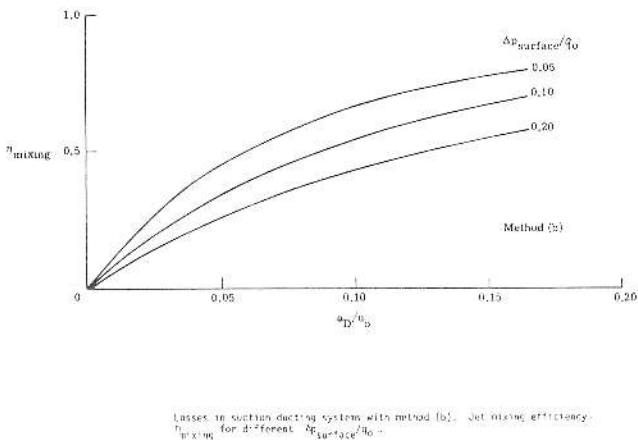


FIGURE 35

Duct mixing- and total energy losses in pressure rise areas can be further reduced: Instead of entering the main spanwise suction ducts the suction air, which is removed from the

external boundary layer at different chordwise locations and total energy levels in the rear pressure rise area, is first mixed to a common total energy level in relatively short mixing ducts. Under the action of jet mixing between the mixing duct- and suction air flow, entering the mixing ducts through flow turning nozzles at higher than local duct flow velocity, the total pressure in the mixing ducts rises according to conservation of mass and momentum. The lower energy suction air, which is removed from the location of lower static pressure on the external surface in the pressure rise area, is then introduced into the area of lower total pressure at the beginning of the mixing ducts, and vice versa (method b', fig. 33a). For a given chordwise pressure rise  $\Delta p/q_0$  across the external surface for a particular spanwise duct the pressure difference between the external surface and the mixing duct is then smaller than with method b. The duct mixing losses decrease accordingly; in addition, the jet mixing efficiency (Figure 37) is higher than with method b. Variations of this approach are feasible.

For a given number of suction ducts the chordwise variation of the total pressure difference of the suction air between the external surface and the suction ducts and the resulting duct mixing losses then decrease approximately by the ratio  $(1 + \eta_{\text{mixing}})^{-1}$ . The jet mixing efficiency  $\eta_{\text{mixing}}$  for method b' is shown in Figure 36.

Alternately, assuming the same duct mixing losses, the chordwise external static pressure variation across a particular duct may be raised by the ratio  $(1 + \eta_{\text{mixing}})$  to allow  $(1 + \eta_{\text{mixing}})^{-1}$  times the number of spanwise ducts.

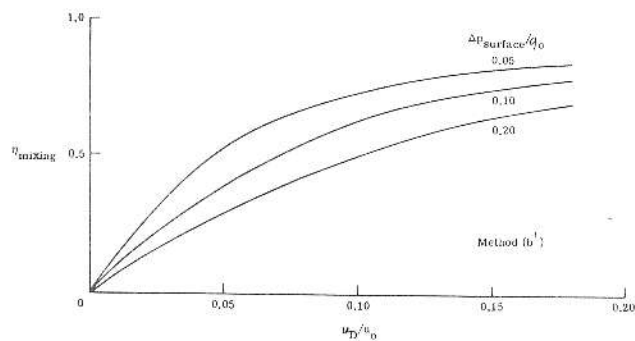


FIGURE 36

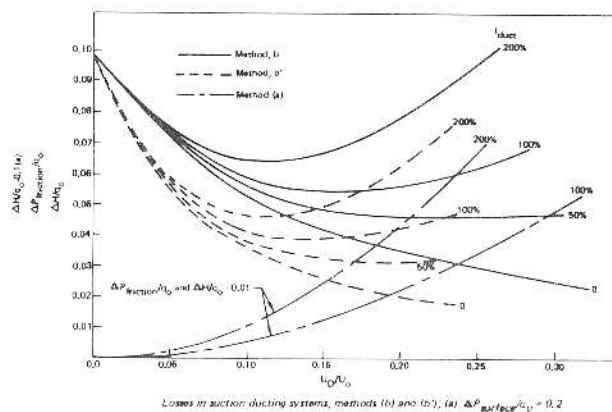


FIGURE 37

### Estimates of duct total energy losses

$$\frac{\Delta H}{q_\infty} = \Delta H / \frac{\rho}{2} U_\infty^2$$

( $U_\infty$  = flight speed) due to duct wall friction and mixing losses are shown in figure 37 versus the ratio  $u_{duct}/U_\infty$  with the methods (a), (b), (b') for an external pressure rise  $\Delta p/q_\infty = 0.20$  across individual ducts and for various duct lengths. Uniform chord and spanwise suction, a linear external pressure rise, constant duct velocity  $u_D$  along the duct, and turbulent pipe friction losses without major secondary flow losses were assumed

$$\left( \frac{\Delta p_{Duct}}{q_{Duct\ end}} = 1 \text{ for } l_D / \text{hydr. } D = 40 \right).$$

Additional duct wall friction losses due to jet mixing of the incoming suction air with the duct flow as well as total energy losses in the external suction skin and inlet flow turning nozzles or vanes were neglected in this simplified analysis.

In view of the smaller duct losses with methods (b) and (b'), as compared to throttling method (a), (fig. 37) primary emphasis is given to the methods (b) and (b'). With increasing duct velocity  $u_D$  the duct friction losses increase approximately proportional to  $u_D^2$  (more accurately  $u_D^{1.8}$  for turbulent duct flow), while the duct mixing losses with methods (b) and (b') (proportional to  $(u_E - u_D)^2$ ) decrease at larger duct velocities  $u_D$  (see fig. 37) as a result of the smaller velocity difference  $u_E - u_D$  between the suction air, entering the duct tangentially at velocity  $u_E$  and the mean duct flow. Accordingly, the jet mixing efficiency  $\eta_{mixing}$  increases with increasing duct velocities  $u_D$  (figs. 35 and 36 show  $\eta_{mixing}$  versus  $u_D/u_\infty$  for different external pressure rises  $\Delta p/q_\infty$  across individual ducts with methods (b) and (b')). The duct total energy losses  $\Delta H_{friction + mixing}$  then minimize at an optimum duct velocity  $u_{D\ opt}/U_\infty$ .

For duct velocities below or above this optimum duct velocity the respective mixing- or duct wall friction losses dominate. For longer ducts, duct friction losses increase, shifting the optimum duct velocity to lower values, and vice versa. In contrast, the duct total energy losses with throttling method (a) increase continuously with increasing duct velocity and are substantially larger than with the more efficient methods (b) and especially (b'). Furthermore, duct total energy losses due to the formation of thick duct wall boundary layers, when the suction air is introduced at a normal angle into the duct through throttling holes, etc., are substantially larger than the conventional turbulent pressure drop in pipes, as verified experimentally.<sup>17</sup> Therefore, throttling method (a) should be used only for smaller values of  $\Delta p_{surface}/q_0$  and at low duct velocities, preferably with holes drilled at an oblique angle to the duct flow to partially recover the momentum of the incoming suction air.

With increasing external pressure rises  $\Delta p_{surface}/q_0$  for individual ducts the duct mixing losses increase, while the duct wall friction losses, on the other hand, decrease as a result of the smaller total duct wetted area and the correspondingly increased duct hydraulic diameter with the fewer larger size ducts for larger ratios  $\Delta p_{surface}/q_0$ . The total duct losses, i.e. the sum of duct friction and mixing losses, increase accordingly with increasing  $\Delta p_{surface}/q_0$ .

Under otherwise the same conditions the optimum duct velocity for minimum duct friction + mixing losses is lower with method (b') than with (b) (fig. 37).

Equal duct mixing losses with methods (b) and (b') result when the pressure differences between the duct and the ex-

ternal surface are equal with both methods. With method b',  $\Delta p_{surface}/q_0$  for a particular duct then increases by the factor  $(1 + \eta_{mix})$  to decrease accordingly the duct number by the ratio  $(1 + \eta_{mix})^{-1}$ . With such fewer ducts turbulent duct wall friction losses (assuming the same total cross-sectional area) decrease by a factor  $(1 + \eta_{mix})^{-0.6}$ ; i.e. for a given sum of duct friction + mixing losses (for the same duct length and cross-sectional area) the number of suction ducts with method (b') may be 40 percent to 45 percent smaller than with method (b). This consideration can become crucially important in simplifying the LFC suction ducting design using method b'.

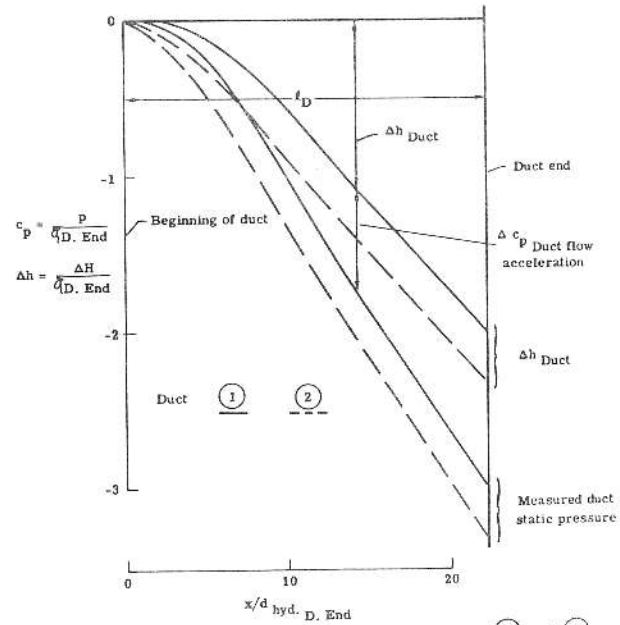
Suction duct experiments by K. Rogers and the author<sup>17</sup> have given the following suction duct total energy losses:

Case 1: Suction air enters duct normal to duct without turning vanes

$$\Delta H_{Duct}/q_{Duct\ end} = 1 \text{ for } l_{duct}/d_{hyd} \text{ at duct end} = 10 \div 12 \text{ (Fig. 38), i.e. } \lambda_{Duct} = 1/10 \div 1/12.$$

Case 2: Suction air enters duct through turning vanes at about duct velocity for

$$\frac{\text{Duct}}{d_{hyd\ Duct\ end}} \cong 40, \text{ i.e. } \lambda_{Duct} \cong \frac{1}{40}$$



Static pressure  $c_p$  and total energy losses  $\Delta h$  in ducts (1) and (2) without duct inlet turning vanes.  $\frac{u_{D, End}}{u} \cdot \frac{l_D}{D} \approx 600/900$ .  
Ref.: Northrop Rep. BLC-22, (1953).  $S_D$  as with duct (1)

FIGURE 38

Case 3: Ideal duct with carefully laid out inlet nozzles, nozzle exit velocity everywhere equal to or close to local duct flow velocity (Figs. 39a-c):

$$\frac{\Delta H_{Duct}/q_{Duct\ exit}}{q_{Duct\ end}} = 1 \text{ for } d_{hyd} \text{ Duct end} = 120 \div 150 (\lambda_D = 1/120 \div 1/150).$$

In other words, a careful aerodynamic design of the suction ducts, minimizing secondary flow and duct wall friction losses, is well worth it in order to reduce suction duct total energy losses.

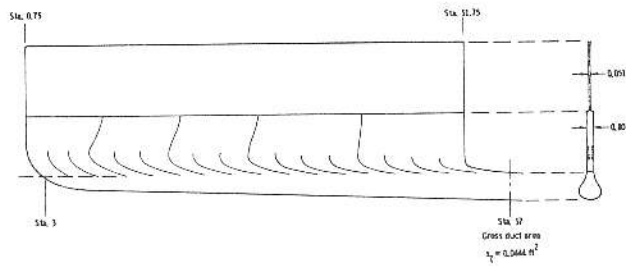
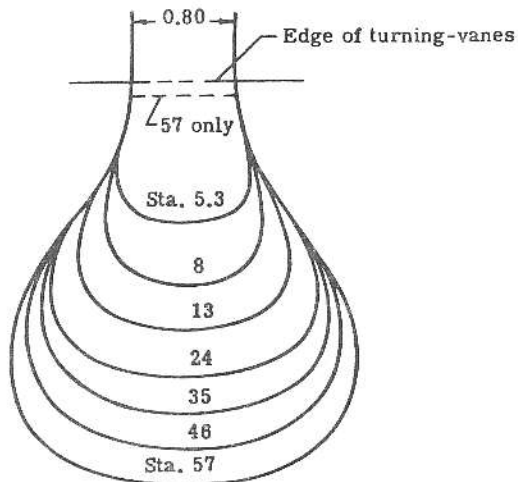
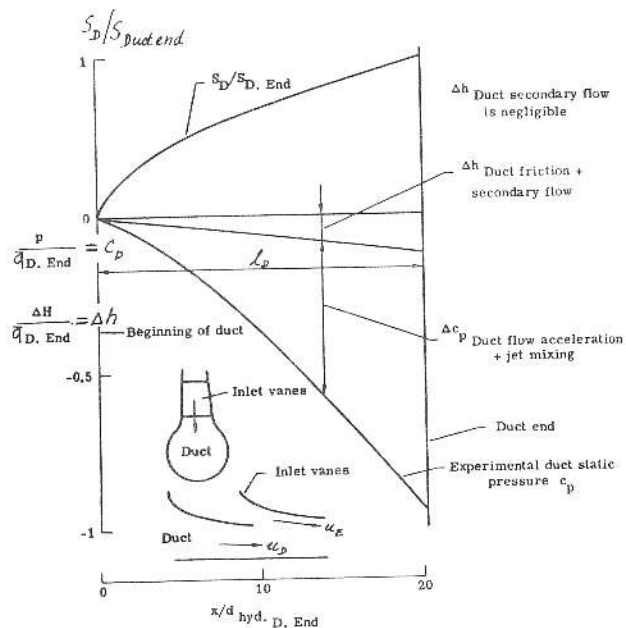


FIGURE 39 C. Improved suction duct (II and III)



Typical cross-sections - improved suction duct (II and III).  
FIGURE 39 B.



Static pressure  $c_p$  and total energy losses  $\Delta h$  in ideal suction duct (II),  $u_E/u_D = 1$  to  $1.08$  along duct,  $\frac{u_{D, End} \cdot L_D}{u_D} = 1.3 \cdot 10^6$ . Duct turning vanes properly sealed (Improved suction duct).  
Ref.: Northrop Rep. NAL-55-547, BLC-70 (1955).

FIGURE 39 A.

The above described duct design considerations have decisively influenced the design parameters of the above described strut-braced 32.4-meter LFC glider, especially the choice of the wing chord ( $c=0.6$  meter) and wing thickness ratio  $t/c = .128$ . The start of the pressure rise on the upper and lower surface was assumed at  $0.7$  and  $0.75c$ , respectively, using suction ducting method  $b'$ .

To reduce the sensitivity against off-design deviations in the chordwise suction distribution a more uniform chordwise  $v_\infty/U_\infty$  distribution appears preferable overall as well as for individual suction chambers. This consideration is particularly important when the rear pressure rise is accomplished over short chordwise distances in the rear part of the airfoils, requiring relatively high area suction velocities within a narrow chordwise zone. Small percentage errors in the local suction rates can then appreciably change the value

$$\left( -\frac{\partial^2 u}{\partial y^2} \right)_0$$

and thus the shape of the boundary layer profile in this zone. Under such conditions, laminar separation, leading to premature transition, can then easily occur with insufficient suction and must be prevented by all means.

In summary, LFC airfoils with a particular low profile drag should preferably be laid out with an extensive region of accelerated flow at design; the rear pressure rise should be located relatively far downstream and should be only slightly concave to enable a reasonably uniform chordwise suction distribution. A small chord trailing edge cruise flap with a concave "corner" with a flexible surface of the Eppler type on the upper surface at the hinge line maximizes the flap down deflection with low profile drag. From the standpoint of a favorable compromise between performance and complexity relatively thin LFC airfoils ( $t/c = .12$  to  $.13$ ) appear attractive for LFC wings of high performance sailplanes.

Figure 40a shows an example of such a LFC airfoil for sailplanes, with the rear pressure rise located downstream of  $0.7c$  and suction concentrated over a short chordwise distance (fig. 40b).

With the direct injection of the suction air into the spanwise ducts for the airfoil P84R, using method  $b$ , the duct wall friction and secondary flow losses are substantially larger (50 percent to 100 percent), as compared to LFC airfoils with the rear pressure rise starting at  $x/c = .7$ , using method  $b'$ . This result is explainable by the larger available duct cross sectional area of the latter type of airfoils and the correspondingly smaller duct velocity and ratio of duct length to diameter, when the rear pressure rise is located far downstream, as well as by the smaller secondary flow losses inherently possible with method  $b'$ , as compared to method  $b$ . In addition, the suction air mixing losses are lower with method  $b'$ . For these reasons, emphasis was finally given to LFC airfoils of the GL6 type (fig. 40), with the rear pressure rise located relatively far downstream, in spite of the additional complexity with the chordwise suction ducting using method  $b'$ .

#### IV. Discussion of Low Drag Suction Methods

The question arises concerning the choice of suitable boundary layer suction methods for suction laminarization in the rear pressure rise area of an LFC wing or fuselage. In principle, laminar flow can be maintained by means of suction through one or several individual slots, or by approaching area suction, removing the innermost slowest boundary layer particles located close to the surface either through closely spaced fine two-dimensional spanwise slots, or through an electron-beam drilled surface with very closely

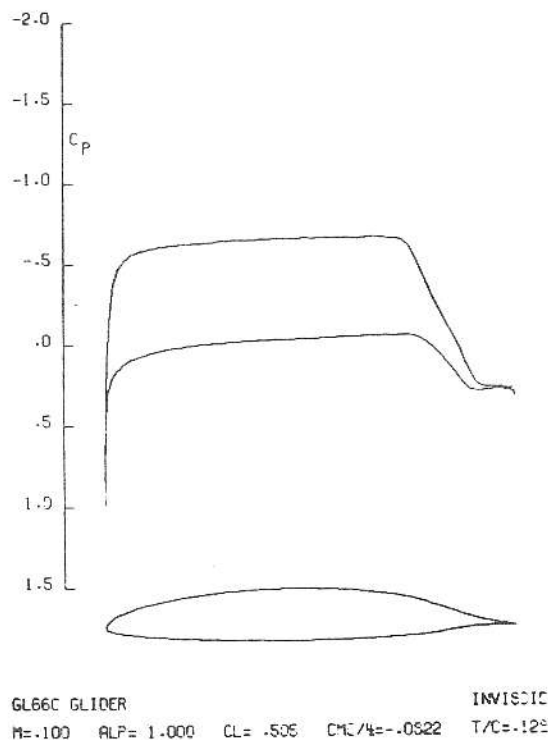


FIGURE 40 A. Glider airfoil GL66C chordwise pressure distribution.

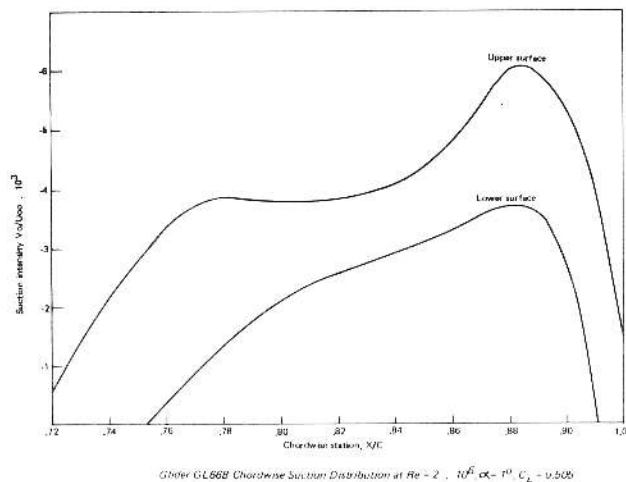


FIGURE 40 B

spaced small diameter holes, or a porous surface. Aerodynamically, area suction, closely approached as described above, is superior over suction through few individual slots, as shown, for example, by comparison LFC experiments by the author in the inlet length of laminar flow tubes at high length Reynolds numbers.<sup>17</sup> Suction through perforated LFC surfaces generates weak streamwise disturbance vortices, which may adversely interfere with amplified boundary layer disturbances of the Tollmien-Schlichting, Taylor-Goertler or crossflow type, unless their centers are located very close to the surface sufficiently far away from the critical layer of such amplified boundary layer disturbance vortices. This is usually the case with an electron-beam drilled surface with very closely spaced small diameter suction holes in the rear pressure rise area of an LFC wing, where the boundary layer is relatively thick.

Using as an example an electron-beam drilled spanwise suction strip, extending over the rear pressure rise area from about  $0.65c$  to the flap hinge at around  $0.9c$ , the average suction velocity ratio on the upper surface is of the order  $\bar{v}_v/U_\infty \cong 0.003$  at  $Re_c = 2.10^6$ . Assuming suction holes of  $0.1$  mm ( $.004''$ ) diameter and a hole pitch of  $0.4$  mm ( $.016''$ ) the surface porosity is 5 percent. The average velocity in the suction hole is then  $\bar{v}_{hole}/U_\infty = .06$ . The corresponding pressure drop through a  $0.5$  mm ( $.020''$ ) thick perforated suction skin with  $d = 0.1$  mm i.d. holes is  $\Delta p_{hole} = 0.05 q_\infty$ , assuming constant diameter holes. Taking into account the taper of the suction holes, inherent with electron-beam drilling, the suction surface pressure drop is somewhat smaller but probably still sufficiently large to dispense with an additional suction metering skin below the perforated skin, which might be needed to maintain sufficiently uniform suction in spanwise direction. This conclusion should not be generalized to higher Reynolds numbers for larger powered LFC airplanes.

Problems arise with the manufacturing of perforated LFC suction strips over long spanwise distances along the entire length of individual wing panels. These strips may be welded together at an angle to the mean flow direction. The figures 33 and 34 show a possible layout of such a suction surface and its ducting in chord- and spanwise direction, together with the mixing ducts.

Clogging of the small electron-beam drilled holes by water and the removal of the water from the suction holes may be a problem at the relatively low flight dynamic pressures of LFC sailplanes and must be studied further.

Using holes of  $0.4$  mm span- and chordwise pitch and  $d = 0.1$  mm diameter the suction pattern repeats itself after a chordwise distance of around  $2$  mm, i.e. area suction is thus rather closely approached. Goldsmith's equivalent slot flow Reynolds number for single row of suction holes (ref. 2) is then  $\bar{u}h/\nu \cong 4$ . This value is somewhat smaller than the values of Head on a perforated vampire LFC glove surface at  $Re_c = 18.10^6$ , i.e. suction hole induced streamwise disturbance vortices should be of no concern for the suction laminarization at the low  $Re_c$ -values of LFC sailplanes. Even at  $Re_c = 4.10^6$ ,  $\bar{u}h/\nu$  would increase only to  $5.6$ , being still conservatively low for this chord Reynolds number and in the absence of sweep induced boundary layer crossflow.

Assuming closely spaced fine spanwise slots as an alternate approach to area suction, the slot flow Reynolds number should preferably be kept below the critical value  $Re_s \equiv (\bar{v}_s/\nu)_{slot} = 100$ ,<sup>17</sup> below which the slot wake flow is purely viscous and steady. With  $\bar{v}_v/U_\infty = 0.003$  at  $Re_c = 2.10^6$  the corresponding slot spacing is  $\Delta x/c = .017$ , or for  $\bar{c} = 0.6m \rightarrow \Delta x = 10mm$ , requiring  $n \geq 12$  slots to laminarize the boundary layer in the rear pressure rise area of the upper surface for  $Re_c = 100$ . For  $Re_c = 4.10^6 \rightarrow \Delta x = 7mm$ , requiring  $n \geq 17$  slots in this zone.

The thickness of the sucked boundary layer is of the order  $0.17$  mm to  $0.20$  mm in the rear pressure rise area of the upper surface, leading to about  $0.20$  mm slot width. Such relatively wide slots are easy to cut with a jeweler's circular saw, as developed by the author's Northrop LFC group, preferably using a lithium-aluminum suction skin sheet. Multiple slot cutting is perhaps possible with such slots.

To maintain structural integrity the slotted suction sheet must be supported by a continuous inner skin, preferably of a lightweight sandwich type in advanced composites, containing suction metering holes and separated from the slotted suction sheet by narrow spanwise plenum chambers, which are needed to establish sufficiently uniform spanwise flow

along each slot.

Figure 34 shows schematically the suction skin of a slotted LFC surface.

The practical feasibility of low drag suction through closely spaced fine slots has been demonstrated in low turbulence tunnels as well as in flight. The practical feasibility of electron-beam drilled LFC surfaces in flight has not yet been sufficiently verified. In spite of this fact electron-beam drilled LFC surfaces appear particularly attractive, provided it is possible to manufacture long electron-beam drilled LFC suction strips in spanwise direction, either in titanium or preferably lithium-aluminum, and provided the water contamination problem of the suction holes can be handled for LFC sailplanes.

## V. Design Consideration of Suction Drive System (Suction Compressor and its Drive Windmill) for an LFC Sailplane

For the time being, a single suction drive windmill was assumed driving the suction compressors of wing, fuselage, etc., through shaft- or perhaps belt drives. This windmill was laid out for flight at  $Re_c = 2.10^6$  and a flight speed  $U_\infty = 38.5$  m/sec at sea level condition, corresponding to flight at  $(l/D_{max}) = 100$  with water ballast. With an optimum suction air exhaust velocity of  $0.85U_\infty$ , assuming a transfer efficiency of 0.85, the windmill drag for the entire 32.4 meter span airplane is 2.78 kg (using the equivalent suction drag to re-accelerate the suction air to  $0.85U_\infty$  including suction drive losses).

A 2-0-2 counterrotating windmill was chosen (4 blades total) to partially recover the windmill rotational slipstream kinetic energy and thereby reduce the windmill induced losses. A high windmill advance ratio at the tip  $\lambda_T = 1$  was chosen to raise the windmill blade chord Reynolds numbers  $Re_{c, Blade}$  thereby minimizing the blade friction losses for a given windmill induced efficiency  $\eta_{ind}$ .

Assuming  $\eta_{ind} = .97$  leads in a straight-forward manner to a Theodorsen-type windmill, using Theodorsen's curves<sup>19</sup> for the mass-coefficient  $\kappa$  and blade circulation function  $K^{19}$  of the 2-0-2 windmill (two front and two rear rotor blades).

The corresponding windmill diameter  $d$  and angular velocity  $\omega$  are  $d = 0.95$  m and  $\omega = 81.05$ /sec. Figure 41 shows the radial variation of the windmill blade chord  $c_{Bl}$ , blade lift coefficient  $C_{L, Blade}$  and blade chord Reynolds number

$$Re_{cBl} = \frac{w_\infty c_{Bl}}{\nu}$$

The blade lift coefficient was chosen slightly below the values for maximum section lift to drag ratio. To minimize blade profile drag losses, rather thin blade sections were assumed, choosing high strength and stiffness materials for the blades. The low blade chord Reynolds numbers will no doubt require artificial control and elimination of laminar separation bubbles, as demonstrated by the author on a 4.8 percent low Reynolds number airfoil at  $c_L = .8^{20}$  and by Mangalam and the author on a 7.3 percent thick more strongly cambered low Reynolds number airfoil at  $c_L = 1.1^{21}$ . This latter airfoil gave a maximum section lift-to-drag ratio of  $Re_c = 90,000$ , and 70 at 70,000, using artificial boundary layer destabilization for elimination of laminar separation bubbles on the upper surface by means of three spanwise narrow tape strips.

Assuming proper artificial control for the elimination of laminar separation bubbles on the upper blade surface an average blade section to lift-to-drag ratio of 76 was assumed, leading to a blade frictional efficiency of the windmill blade  $\eta_{fr} = .971$  and  $\eta_{windmill} = .942$ .

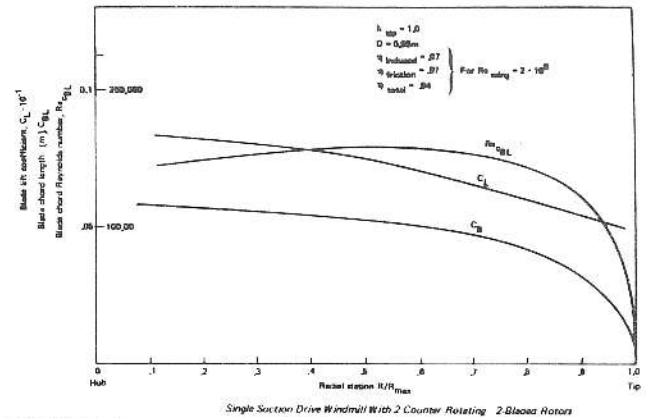


FIGURE 41

Wider chord blades and correspondingly larger blade chord Reynolds numbers are possible by lowering the windmill induced efficiency  $\eta_{ind}$  to, for example, 0.96.  $\eta_{friction}$  increases then slightly to .973. The higher induced losses, though, reduce  $\eta_{windmill}$  to .934.

Next, the main LFC suction compressor was laid out, handling the suction air of the inboard  $2/3$  half span of the wing, preceded by one or two booster stages. The latter raise the total pressure of the suction air of the upper surface with the lowest total pressure in the upstream zone of the rear pressure rise to the level of the suction air of the lower surface and of the upper surface in the most downstream zone of the pressure rise.

At  $Re_c = 2.10^6$  the corresponding suction volume rate  $Q_a$  and suction compressor pressure rise are  $Q_a = 0.272$  m<sup>3</sup>/sec and  $\Delta p_g = 100$  kg/m<sup>2</sup>. Assuming a compressor tip speed  $U_T = 75$  m/s leads to a compressor pressure rise coefficient  $\psi_T = .284$ . With a mass flow coefficient  $\phi_T = 0.4$  the meridional flow velocity is 30 m/sec, leading to a compressor diameter  $D = .129$  meters, assuming a hub to tip radius ratio 0.55. Exit stator blades turn the flow back into axial (i.e. flight) direction.

Selecting six rotor blades and  $c_L = .6$  at the blade tip leads to a blade tip chord of 0.035 m and a blade tip chord Reynolds number

$$\left(\frac{w_\infty c}{\nu}\right)_{tip} = 186,000.$$

The corresponding values at the hub, assuming  $C_{L, hub} = 0.8$ , are  $c_{Hub} = .046$  m and  $Re_{c, Hub} = 140,000$ . The blade span is  $b = 0.029$  m, leading to a rotor blade aspect ratio of 0.725. Higher blade aspect ratios, of course, would be possible by increasing the blade number, leading to blade aspect ratios of the order 1, at the cost of lower  $Re_c$ 's and correspondingly somewhat larger blade friction losses. There is nothing wrong with low compressor rotor blade aspect ratios of the order 1, as shown by de Haller in the 1940's as well as independently by Pratt and Whitney.

As with the windmill the low compressor blade chord Reynolds numbers will need a careful control of laminar separation bubbles on the upper blade surface.

Smaller hub to tip radius ratios ( $\cong 0.42$ ) could be feasible by using inlet stator blades and locating them on a large radius in the suction duct exit areas, similar to Kaplan- or Francis turbines. With such inlet flow prerotation the relative flow deceleration on the rotor blade at the hub is correspondingly reduced to allow substantially smaller hub radii without excessive relative flow deceleration. The blade span

increases then accordingly to enable further increased blade chords and Reynolds numbers to lower accordingly the blade frictional losses. The losses of the inlet stator blades, located at a large radius in the field of low flow velocity, are rather insignificant. In essence, the suction compressor must deliver a certain pressure rise combined with a reasonably high meridional exit velocity.

The compressor stage efficiency was estimated from an extrapolation of the Haller's best single stage experimental axial flow compressors, using NACA 65 type bladings with carefully designed fairings between the blade and hub. At a blade chord Reynolds number of 340,000 de Haller had measured in the 1940's a stage efficiency of up to 94 percent. One might thus extrapolate to stage efficiencies of 91 percent to 92 percent for the above described suction compressor, taking into account the possibility that further improved blade sections with a better control of laminar separation bubbles at lower  $Re_c$ 's should now be possible.

Still higher suction compressor efficiencies appear feasible with inlet stator blades, located at a large radius, as discussed above, and particularly with counterrotating rotor bladings, approaching perhaps  $\eta_{sc} = .93$ . Transfer efficiencies  $\eta_T = \eta_{windmill} \times \eta_{suction\ compressor}$  beyond 0.85 appear thus feasible.

The suction compressor and its drive windmill were designed individually as optimal as possible, leading to a 14 to 1 gear ratio between these components. Highly efficient and lightly loaded, though, relatively heavy gears are then needed to minimize gearing losses. Belt drives between the windmill and suction compressors, using advanced modern materials for the belts, represent an alternate suction compressor drive method.

A direct drive between the windmill and the suction compressor with a satisfactory transfer efficiency could in principle, be possible by using a counterrotating windmill on each wing side, with  $\lambda_T \sim 0.5$  to  $0.7$ , driving a slowly running multi-stage counterrotating axial flow compressor, operating at a high degree of reaction above 1 to maximize the work output per stage.

Since the nondimensional suction flow rates vary substantially with Reynolds number  $Re_c$  and  $c_l$  for the vastly different flight conditions of a high performance LFC sailplane adjustable suction compressor rotor blades appear highly desirable. Adjustable pitch for the windmill blades may not be needed; detailed studies, though, are necessary over the entire range of flight conditions to confirm this.

The suction drive system might be used to improve the sailplane performance under poor soaring conditions as follows: The suction drive windmill can be geared to an electric generator (via a clutch), which can operate also as an electric motor. Under favorable soaring conditions the windmill can drive this generator to charge up batteries or fuel cells. When soaring conditions become marginal the batteries can drive the generator as a motor, and the windmill will then operate as a propeller to overcome a large percentage of the airplane drag, perhaps 100 percent. For this purpose the windmill blades would have to be designed for smaller blade lift coefficients, probably using a trailing edge cruise flap for the blades to maintain high blade section lift to drag ratios both as a windmill as well as a propeller. Adjustable pitch would then be needed for the windmill blades.

During normal soaring conditions the electric generator would be declutched.

To qualify as a sailplane, the charge of the batteries or fuel cells at landing should not be lower than at takeoff.

## ACKNOWLEDGEMENT

The author is greatly indebted to Jeffrey K. Viken, who has conducted the KG-analysis as well as the boundary layer development and stability analysis of the LFC airfoils discussed in the report. Furthermore, the author wishes to express his appreciation to W. T. Hodges for his help in preparing the figures.

## REFERENCES

1. Pfenninger, W.: Untersuchungen ueber Reibungsverminderungen an Tragfluegeln insbesondere mit Hilfe von Grenzschichtabsaugung." Mitteilung 13, Institute for Aero, Zuerich, 1946. English Translation NACA TM 1181 (1947).
2. Goldsmith, J.: Critical Laminar Suction Parameters for Suction into an Isolated Hole or a single Row of Holes. Northrop Report BLC-95, NAI-57-529, (February 1957).
3. Pfenninger, W.; Reed, H.L.; and Dagenhart, J.R.: Design Considerations of Advanced Supercritical Low Drag Suction Airfoils. Viscous Flow Drag Reduction. Vol. 72 of Progress in Astronautics and Aeronautics, (1980).
4. Pfenninger, W.: Experiments With a 15 Percent Thick Slotted Laminar Suction Wing Model in the NACA Langley Low Turbulence TDT-Tunnel. AFTR 5982, (1951).
5. Pfenninger, W.: Experiments on a Laminar Suction Airfoil of 17 Percent Thickness. IAS-Journal, volume 16, number 4, (1949).
6. Pfenninger, W.; and Groth, E.: Low Drag Boundary Layer Suction Experiments in Flight on a Wing Glove of an F94A Airplane With Suction Through a Large Number of Fine Slots. Boundary Layer and Flow Control, G. V. Lachmann, Editor, volume 2, page 98, (1961).
7. Gross, L.W. and Pfenninger, W.: Experimental and Theoretical Investigation of a Reichardt Body of Revolution With Low Drag Suction in the NASA Ames 12 Foot Pressure Wind Tunnel. Northrop Report Number NOR-63-46, BLC 148, (1963).
8. Goldsmith, J.: Laminar Flow at the Junction of Two Airplane Components. Boundary Layer and Flow Control, volume 2, G.V. Lachmann, Editor, pp. 1000-1006, (1961), Pergamon Press.
9. Kuettner, J.: Soaring in Thermal Waves. Lecture presented to Soaring Society of America, San Diego; March 1, (1985).
10. Kuettner, J.: Vertical Motions in the Jetstream. 7th OSTIV Congress, Poland; (June 1958).
11. Pfenninger, W.: Dynamic Soaring in the Jetstream With all Laminar High Performance LFC Airplanes. 18th OSTIV Congress, Hobbs, (1983).
12. Ackeret, J.: Probleme des Flugzeugantriebs in Gegenwart und Zukunft. Schweiz Bauzeitung, Bd, 111, p. 237, 1938.
13. Viken, J.: George Washington University Master's Thesis, (1980).
14. Pfenninger, W.: Design Considerations of Large Global Range High Subsonic Speed LFC Transport Airplanes. AGARD Vki Special Course on Concepts for Drag Reduction, AGARD Report 654, Rhode-St. Genese, Belgium, (1977).
15. Jameson, W.: The Wandering Albatross. Rupert Hart-Davis, London, 1958.
16. Schuemann, Will: A New Wing Planform with Improved Low-Speed Performance. Soaring Magazine, (February 1983).
17. Pfenninger, W.: USAF and Navy sponsored Northrop LFC Research Between 1949 and 1967. AGARD/VKI Special Course on Concepts for Drag Reduction, Rhode-St. Genese, Belgium, AGARD Report 654, (1977).
18. Pfenninger, W.: Some General Considerations of Losses in Boundary Layer Suction Ducting Systems. Northrop Report BLC-29, (February 1954).
19. Theodorsen, T.: Theory of Propellers (1948). Theory of Propellers I. NACA TR-774 (1944).
20. Pfenninger, W.: Experimental Investigation of an Airfoil with High Lift to Drag Ratios at Low Reynolds Numbers. Northrop Report BLC-84, NAI-56-188, 1956.
21. Mangalam, S. and Pfenninger, W.: Wind Tunnel Tests on a High Performance Low Reynolds Number Airfoil. AIAA 13th Aerodynamic Testing Conference, March 1984. AIAA Paper 84-0628.